Shi et al. *Zool. Res.* 2025, 46(5): 1009−1028
https://doi.org/10.24272/j.issn.2095-8137.2025.093
https://cstr.cn/32248.14.zr.2025.093

ZR | Zoological Research

Article Open Access

Epigenetic regulation and maternal-to-zygotic transition in dwarf surf clam (*Mulinia lateralis*): Insights from chromatin state profiling and transcriptomics

Jia-Le Shi[1,2], Jia-Xiang Liu[1,2], Zhong-Cheng Wei[1], Miao-Miao Yin[1,2], Zu-Jing Yang[1], Jing-Jie Hu[1,2], Zhi Ye[1,2,*], Zhen-Min Bao[1,2]

[1] *MOE Key Laboratory of Marine Genetics and Breeding*, *College of Marine Life Sciences*, *Ocean University of China*, *Qingdao*, *Shandong* 266003, *China*

[2] *Key Laboratory of Tropical Aquatic Germplasm of Hainan Province*, *Sanya Oceanographic Institution*, *Ocean University of China*, *Sanya*, *Hainan* 572024, *China*

ABSTRACT

Bivalve mollusks represent a taxonomically and economically significant clade within Mollusca. However, the regulatory mechanisms governing their embryonic development remain poorly characterized. The dwarf surf clam (*Mulinia lateralis*), characterized by a short generation time and high fecundity, has recently gained recognition as an ideal model system for bivalve embryological research. This study explored the epigenetic mechanisms driving embryogenesis in *M. lateralis*, with a particular focus on the maternal-to-zygotic transition (MZT), by integrating chromatin-state profiling and transcriptomic analysis. For the first time in this species, CUT&Tag was employed to generate high-resolution landscapes of histone modifications H3K4me1, H3K4me3, H3K27me3, and H3K27ac across key developmental stages. The resulting data revealed extensive reprogramming of histone marks, indicating dynamic shifts in chromatin architecture during early embryonic development. Integration with transcriptomic data identified the timing of MZT in *M. lateralis* between the morula and gastrula stages and highlighted a suite of candidate genes essential for embryogenesis. These findings provide mechanistic insight into chromatin-mediated control of bivalve embryogenesis and establish *M. lateralis* as a robust platform for epigenomic research in marine invertebrates, with implications for functional gene studies and aquaculture advancement.

Keywords: *Mulinia lateralis*; CUT&Tag; Histone modifications; Epigenetic regulations; Maternal-to-zygotic transition

INTRODUCTION

Chromatin organization in eukaryotes is governed by nucleosome-based architecture that enables efficient DNA packaging while permitting dynamic regulation of gene expression. This regulatory plasticity is orchestrated through epigenetic mechanisms, including DNA methylation, histone post-translational modifications, and chromatin remodeling (Eichten et al., 2014; Turner, 2007). These modifications control gene expression without altering the DNA sequence, primarily through changes in chromatin accessibility and structure (Eichten et al., 2014). Among these, histone modifications represent a particularly complex and informative layer of epigenetic regulation. Through chemical alterations, such as methylation, acetylation, and phosphorylation, histone tails serve as dynamic platforms for the recruitment of regulatory proteins and remodeling complexes, thereby shaping transcriptional outcomes (Bannister & Kouzarides, 2011; Millán-Zambrano et al., 2022; Turner, 2007). Multiple histone modifications have been identified, with several serving as critical determinants of chromatin states and as markers of cis-regulatory elements, particularly within non-coding genomic regions (Millán-Zambrano et al., 2022). H3K4me3 is typically enriched at actively transcribing promoters, while H3K4me1 and H3K27ac are predominantly associated with active enhancers and H3K27me3 is linked to repressive chromatin regions (Blayney et al., 2023; Millán-Zambrano et al., 2022). These epigenetic signatures not only delineate the functional organization of chromatin but also enable the identification of regulatory elements that modulate gene expression, including promoters and distal enhancers in

Received: 29 May 2025; Accepted: 21 July 2025; Online: 22 July 2025

Foundation items: This work was supported by the National Natural Science Foundation of China (32200667), Shandong Provincial Special Funds for Taishan Scholars (tsqn202306104), Hainan Province “South China Sea New Star” Science and Technology Innovation Talent Platform Project (NHXXRCXM202365), and Hainan Provincial Joint Project of Sanya Yazhou Bay Science and Technology City Grant (2021JJLH0090)

*Corresponding author, E-mail: yezhi@ouc.edu.cn

non-coding domains (Blayney et al., 2023). Understanding these chromatin-based regulatory mechanisms is fundamental for deciphering the complex transcriptional networks that drive embryonic development.

Precise gene regulation during embryogenesis is essential for guiding cell identity establishment and organismal architecture, with histone modifications playing key roles in this process (Bannister & Kouzarides, 2011; Schulz & Harrison, 2019; Turner, 2007). In the earliest stages of embryonic development, gene expression is predominantly governed by maternally inherited mRNAs and proteins. As development progresses, transcriptional control shifts to the embryonic genome through a process known as maternal-to-zygotic transition (MZT) (Schulz & Harrison, 2019), a critical developmental milestone involving extensive genome remodeling and epigenetic reconfiguration to ensure proper expression patterns for cell fate determination (Schulz & Harrison, 2019; Xia et al., 2019). Although the timing, regulatory architecture, and molecular basis of the MZT have been extensively characterized in model organisms such as *Drosophila*, zebrafish, and mice (Sotomayor-Lugo et al., 2024; Vastenhouw et al., 2019), they exhibit significant interspecies variability that does not align with evolutionary relatedness (Fukushima et al., 2023; Vastenhouw et al., 2019). Distinct global patterns of histone modifications before and during zygotic genome activation (ZGA) have been documented in humans, mice, zebrafish, *Xenopus*, *Drosophila*, and *Caenorhabditis elegans*, highlighting the evolutionary plasticity of chromatin regulation during early embryogenesis (Lindeman et al., 2011; Millán-Zambrano et al., 2022; Vastenhouw et al., 2019; Xu et al., 2021).

Despite its importance, the regulatory dynamics of the MZT remain largely unexplored in bivalves, a diverse and evolutionarily distinct class within Mollusca noted for their specialized life history strategies and morphological diversity. Bivalve development follows a biphasic trajectory, with pelagic larval stages transitioning to sessile benthic adults, representing an important model system for studying marine invertebrate ontogeny (Wang et al., 2020). However, the molecular mechanisms governing embryogenesis in bivalves, particularly at the level of epigenetic control, remain poorly understood. Bivalves typically follow an indirect developmental process, with the trochophore stage serving as a critical and evolutionarily conserved larval form observed across numerous marine taxa. This stage is characterized by specialized morphogenetic processes and functional adaptations essential for larval dispersal and survival (Wang et al., 2020). As protostomes, bivalves exhibit mosaic development defined by spiral cleavage and deterministic cell fate specification, whereby embryonic fates are established early and remain fixed, in contrast to regulative development observed in other taxa (Drozdov et al., 2023). In addition to their biological significance, bivalves contribute over 20% of global aquaculture output (FAO, 2024), with taxa such as scallops, oysters, mussels, and clams serving as a high-yield protein source characterized by rapid growth, prolific reproduction, and broad environmental tolerance (Vaughn & Hoellein, 2018). Dissecting the epigenetic mechanisms that regulate their embryogenesis, particularly histone modifications, will not only advance our understanding of their complex regulatory networks but also provide a theoretical basis for enhancing breeding strategies, improving larval survival, and increasing environmental resilience. As such, advancing epigenetic research in bivalves stands to yield both mechanistic understanding and applied benefits across developmental biology and marine biotechnology.

Mulinia lateralis has emerged as a powerful model for bivalve developmental studies due to its short generation time and transparent larval stages that enable high-resolution imaging and experimental manipulation (Yang et al., 2021). To investigate the epigenetic mechanisms orchestrating early embryogenesis in this species, Cleavage Under Targets & Tagmentation (CUT&Tag) was employed to generate genome-wide profiles of key histone modifications (H3K4me1, H3K4me3, H3K27me3, and H3K27ac) across developmental stages. These chromatin maps were integrated with transcriptomic datasets to identify candidate regulatory genes potentially driving embryonic development. CUT&Tag, a highly sensitive method requiring minimal input material, presents a cost-effective and scalable alternative to traditional ChIP-seq for chromatin profiling (Kaya-Okur et al., 2019, 2020). This study aimed to construct a comprehensive epigenomic landscape of *M. lateralis* embryogenesis, with a focus on the MZT, a critical window of regulatory reprogramming. It was hypothesized that temporally dynamic, stage-specific patterns of histone modification correspond to chromatin state transitions that coordinate embryonic gene regulation. The findings of this study are expected to inform both fundamental developmental biology and practical applications in bivalve aquaculture.

MATERIALS AND METHODS

Spawning induction, fertilization, larval culture, and sample collection

The *M. lateralis* specimens used in this study were obtained from the Laboratory of Marine Genetics and Breeding, Ocean University of China, Qingdao, China. No field permissions were required for animal collection in this study. All experimental protocols described in this paper were conducted in compliance with institutional, national, and international guidelines.

Sexually mature male and female individuals were shade-dried for 2 h and subsequently transferred to 500 mL crystallizing dishes containing sterile-filtered seawater (FSW) maintained at 26–27°C with a salinity of 27–28 ppt to induce spawning (Yang et al., 2021). Spawning behavior was closely monitored, and upon initiation of sperm or egg release, individuals were immediately removed, rinsed with FSW, and placed in separate culture dishes to continue gamete release. Sex identification was based on gamete morphology, with sperm appearing as white flocculent aggregates and eggs appearing as yellow granular structures at the bottom of the dish. Following gamete collection, eggs were washed with FSW and filtered through a 150-mesh nylon screen layered above a 500-mesh nylon screen to remove impurities. Sperm was collected using a pipette and transferred to a 50 mL centrifuge tube for subsequent procedures.

Artificial fertilization was conducted at a sperm-to-egg ratio of 3:1. After fertilization, excess sperm were removed using a 500-mesh nylon screen, and the fertilized eggs were incubated in FSW at 21–22°C. Samples were collected at eight developmental stages: zygote (10 min post-fertilization), 4-cell stage (1-h post-fertilization, hpf), morula (2 hpf), blastula (4 hpf), gastrula (6 hpf), trochophore (10 hpf), veliger stage (14 hpf), and D-shaped larvae (18 hpf). The collected samples

were flash-frozen in liquid nitrogen and stored at −80°C for subsequent experiments.

CUT&Tag experiment and data analysis

Nuclei were extracted from flash-frozen samples following previously described protocols (Kaya-Okur et al., 2019). CUT&Tag libraries were prepared using the Illumina Hyperactive Universal CUT&Tag Assay Kit (Vazyme, #TD903, China), with approximately 10 000 nuclei per sample. Two biological replicates were included for each developmental stage. Antibodies targeting four histone marks (H3K4me1, H3K4me3, H3K27me3, and H3K27ac), along with a non-specific IgG control, are listed in Supplementary Table S1. Rabbit IgG (Abcam, ab172730, UK) served as a negative control alongside the histone mark-specific antibodies to assess non-specific background signal, as it does not recognize any particular histone modifications or chromatin-associated proteins. The absence of signal enrichment in the IgG control validated the specificity of antibody binding and supported the reliability of the CUT&Tag peaks identified in the experimental samples (Kaya-Okur et al., 2019). Sequencing of the prepared CUT&Tag libraries was conducted on the Illumina NovaSeq 6000 platform (USA) by Novogene (China).

Raw sequencing reads were processed using the NGS QC Toolkit v.2.3 (Patel & Jain, 2012) to generate high-quality clean reads. Given the structural complexity and repetitive content of the *M. lateralis* genome, reads were aligned to the reference genome (unpublished) using BWA-MEM v.0.7.17 (Li, 2013). The resulting SAM files were filtered by fragment length using the *awk* command, and duplicate BAM files were merged for downstream analysis. Peaks were identified using MACS2 v.2.2.7.1 (Feng et al., 2012) with the parameters: macs2 callpeak -t A.bam -c IgG.bam -f BAMPE --outdir .../... -B -n A -g 1.44e9 --keep-dup auto -q 0.01. Mapping statistics are presented in Supplementary Table S2.

Peak annotation and visualization were conducted using R packages GenomicFeatures (Lawrence et al., 2013), ChIPseeker (Yu et al., 2015), and ggplot2 (Wickham, 2011), along with Integrative Genomics Viewer (IGV) v.2.15.2. Additional analyses, including fragment size distribution, reproducibility of duplicate samples, peak signal enrichment heatmaps, and peak distribution across genomic regions (Figure 1) were performed using an established R pipeline (Kaya-Okur et al., 2019, 2020).

Chromatin state analysis

Chromatin states across key embryonic stages in *M. lateralis* were analyzed using ChromHMM v.1.26 (Ernst & Kellis, 2017), which integrates combinatorial histone modification patterns to infer chromatin states. The model was trained on four histone modifications (H3K4me1, H3K4me3, H3K27me3, and H3K27ac). Initially, aligned BAM files were binarized using the BinarizeBam module in ChromHMM, with a bin size of 200 bp and a signal detection *P*-value threshold of 0.0001. Subsequently, the LearnModel module was used to train the binarized data and infer 10 distinct chromatin states, using a convergence threshold of 0.001. Finally, the genomic locations of the predicted chromatin states were annotated and visualized using IGV v.2.15.2.

Transmission electron microscopy (TEM) and quantitative analysis

Embryos were first fixed in 2.5% glutaraldehyde for 24 h, washed three times with 1× phosphate-buffered saline (PBS), and post-fixed in 1% osmic acid at 4°C for 2 h. The samples were then sequentially dehydrated with 50%, 70%, and 90% ethanol, followed by a gradual substitution with 90% acetone (HUSHI, China), with all steps performed at 4°C. The samples were subsequently treated with 100% acetone at room temperature three times (15 min each) to ensure complete dehydration. The dehydrated tissues were embedded in epoxy resin (EPON 812, China) and sequentially polymerized at 37°C, 45°C, and 60°C for 24 h. Ultrathin sections (70 nm) were prepared using an EM UC7 ultramicrotome (Leica, Germany), stained with uranyl acetate and lead citrate, and examined using a JEM-1200EX transmission electron microscope (JEOL, Japan).

Quantitative analysis of nuclear ultrastructure was conducted using ImageJ v1.54 in conjunction with the Illumination Bias plugin (http://sites.imagej.net/Julien.pontabry/plugins/), following Laue et al. (2019). Nuclear boundaries were manually delineated, and electron-dense versus non-electron-dense regions were segmented using the maximum entropy thresholding algorithm. Electron-dense particles with a minimum size of 0.03 μm^2 were automatically selected and counted. For each image, both the number and total area of electron-dense particles were measured and normalized to the total nuclear area to generate standardized metrics for comparative analysis (Laue et al., 2019).

Immunofluorescence

Embryos were fixed in 4% paraformaldehyde (PFA) at 4°C overnight. Immunofluorescence staining was performed as described in previous research (Laue et al., 2019). Fixed embryos were washed with PBST, incubated overnight at 4°C with primary antibodies, and washed three times in PBST. Secondary antibodies were then applied and incubated overnight at 4°C, followed by another round of three PBST washes. DAPI staining was performed for 30 min, followed by three washes with PBST before imaging under a fluorescence microscope.

Primary antibodies were identical to those used in the CUT&Tag experiment (Supplementary Table S1). Atto488-conjugated secondary antibodies were prepared by conjugating goat anti-rabbit immunoglobulin G (IgG) (Abcam, ab6702, UK) with the Atto488 Conjugation Kit (Fast)-Lightning-Link® (Abcam, ab269896, UK).

RNA sequencing (RNA-seq) and transcriptomic analysis

RNA-seq was performed across eight developmental stages of *M. lateralis*, each represented by three biological replicates. Total RNA was extracted using the RNAprep Pure Tissue Kit DP431 (Tiangen, China) and treated with DNase I (Takara Bio, Japan) to remove genomic DNA. RNA concentration and purity were assessed using a Nanovue Plus spectrophotometer (GE Healthcare, USA), and RNA integrity was confirmed by agarose gel electrophoresis. RNA libraries were prepared using the NEBNext® Ultra™ RNA Library Prep Kit for Illumina® (NEB, USA), with mRNA enrichment performed by poly-T oligo-attached magnetic bead selection to generate poly(A)+ RNA libraries. Libraries were sequenced on the Illumina NovaSeq 6000 platform (USA) by Novogene (China), with 6 GB of raw data per sample.

Raw reads were quality filtered using the NGS QC Toolkit v.2.3 (Patel & Jain, 2012) to obtain clean reads (Supplementary Table S3**)**. High-quality reads were aligned to the reference genome using STAR v.2.7.11b (Dobin et al.,

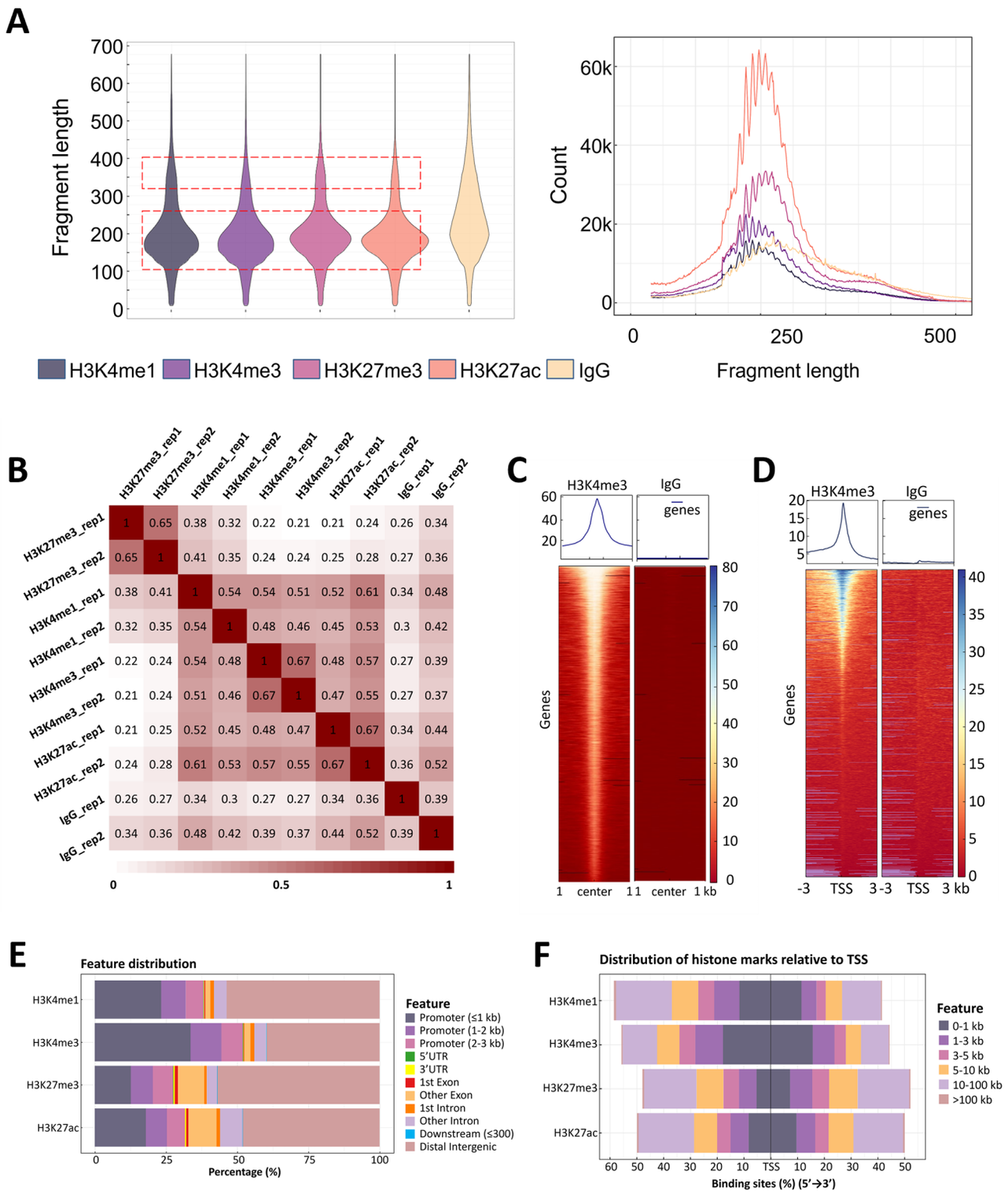

Figure 1 Quality assessment of CUT&Tag in *Mulinia lateralis* embryos at the trochophore stage

A: Fragment size distribution: Plots showing proportion (left) and count (right) of DNA fragments by size. Histone modification samples exhibited strong enrichment of mononucleosome-sized fragments, while control samples displayed a random distribution. B: Replicate reproducibility: High correlation was observed between replicates of histone modification samples, confirming the reproducibility of CUT&Tag. C: Peak signal enrichment: Heatmaps (bottom) and plots (top) showing signal enrichment and random distribution within ±1 kb of CUT&Tag peak for histone modification (H3K4me3) and control (IgG) samples, respectively. D: H3K4me3 enrichment at TSS: Heatmaps (bottom) and plots (top) showing enrichment of H3K4me3 near TSS (±3 kb), with no enrichment observed in IgG control sample. E: Distribution of histone modification peaks across gene structural elements. F: Proportion of histone modification peaks by distance to the TSS.

2013), and gene-level quantification was performed with featureCounts (Liao et al., 2014). Transcript abundance was normalized as transcripts per million (TPM), and statistical analyses were conducted using GraphPad Prism v.8.0.2.

Sample reproducibility was evaluated using both principal component analysis (PCA) for global expression pattern

clustering and Spearman's correlation coefficients for pairwise similarity between biological replicates. Differential gene expression was analyzed using the DESeq2 package (Love et al., 2014) in Rstudio (v.4.2.1), with thresholds set at |Fold Change|>2 and a false discovery rate (FDR)-adjusted *P*-value<0.05. Functional enrichment of differentially expressed genes (DEGs) was conducted using Kyoto Encyclopedia of Genes and Genomes (KEGG) pathway analysis implemented in the clusterProfiler R package (Yu et al., 2012).

Weighted gene correlation network analysis (WGCNA)

WGCNA was performed to identify modules of highly correlated genes across different developmental stages of *M. lateralis*. Genes with zero TPM in all samples were excluded to minimize noise from non-expressed genes. The WGCNA package in R (Langfelder & Horvath, 2008) was used to construct a gene co-expression network. Initially, hierarchical clustering (hclust) was applied to detect potential sample outliers. Soft-thresholding power was determined using the pickSoftThreshold function to establish scale-free topology (soft threshold=20).

An adjacency matrix was constructed to define gene co-expression relationships, and modules containing at least 800 genes were identified using the cutreeDynamic algorithm. Modules were visualized using Cytoscape (v.3.6.1), with the 30 most highly connected genes in each module highlighted in heatmaps. Functional annotation was performed using KEGG pathway enrichment via clusterProfiler in R (Yu et al., 2012), with significantly enriched pathways identified at $P<0.05$ (Supplementary Table S4).

Identification of EZH homologs, phylogenetic analysis, and multiple sequence alignment

To identify homologs of EZH1 and EZH2, protein sequences from various species, including *Homo sapiens*, *Mus musculus*, *Gallus gallus*, *Xenopus laevis*, *Xenopus tropicalis*, *Oryzias latipes*, *Danio rerio*, *Chionoecetes opilio*, *Amphibalanus Amphitrite*, *Drosophila melanogaster*, *Mytilus edulis*, *Mytilus galloprovincialis*, *Mizuhopecten yessoensis*, and *Patella vulgata*, were retrieved from the NCBI and Ensembl databases. Specific protein sequences and Accession IDs are provided in Supplementary Table S5.

Candidate EZH homologs in *M. lateralis* were identified by a BLAST search against the *M. lateralis* protein database, with an *E*-value threshold of <1E-5. Predicted homologous proteins were validated by detecting conserved domains using the SMART tool (https://smart.embl.de/) (Schultz et al., 1998). Phylogenetic analysis of the EZH1 and EZH2 protein sequences was conducted using the neighbor-joining method with 1 000 bootstrap replicates. Multiple sequence alignments were conducted using Clustal W in MEGA v.11 (Tamura et al., 2021). The resulting phylogenetic tree was visualized using iTOL (https://itol.embl.de/) (Letunic & Bork, 2021).

Integrated analysis of CUT&Tag and transcriptome data

H3K4me3 is a well-established marker of actively transcribed gene promoters, H3K27me3 is associated with polycomb repressive complex 2 (PRC2)-mediated silencing, and H3K27ac marks regions of open chromatin, particularly active enhancers when co-localized with H3K4me1 (Jiao & Liu, 2015; Zhu et al., 2023). To integrate CUT&Tag and transcriptome data, "bedtools intersect" (Quinlan, 2014) was used to identify genomic loci modified by specific histone marks. Genes were classified as actively transcribed if they met three criteria: average TPM≥1, presence of overlapping H3K27ac and H3K4me3 peaks (≥1 bp), and absence of H3K27me3 peaks within the promoter region, defined as a ±3 kb window centered on the transcription start site (TSS). This combinatorial chromatin signature reflects accessible promoter architecture conducive to active transcription, while the absence of H3K27me3 indicates a lack of polycomb-mediated repression. The TPM≥1 threshold was applied to eliminate low-abundance transcripts and ensure biological relevance. This integrative approach offers a more reliable and functionally meaningful classification of gene activity across developmental stages. KEGG pathway enrichment analysis was performed on these genes to identify significantly enriched pathways ($P<0.05$). Genes exhibiting at least 1 bp overlap between H3K4me1 and H3K27ac peaks, without H3K27me3 peak overlap, were defined as genes modified by active enhancer markers at specific developmental stages. Gene expression comparisons across stages were analyzed using GraphPad Prism v.8.0.2, and statistical differences were evaluated by two-tailed *t*-tests. Statistical significance was defined as: *: $P<0.05$; **: $P<0.01$; ***: $P<0.001$.

RESULTS

Establishment and validation of CUT&Tag in *M. lateralis*

To optimize CUT&Tag for *M. lateralis*, two critical modifications were introduced to adapt the standard protocol to the biological and genomic characteristics of this species. First, nuclei were used instead of dissociated cells to overcome challenges associated with cell dissociation and to mitigate osmotic imbalances between marine invertebrate cells and standard buffers. This approach also reduced variability in cell-type representation across developmental stages caused by differential dissociation efficiency. Second, due to the high structural complexity and repeat content of the *M. lateralis* genome, Bowtie2—originally recommended for CUT&Tag—yielded low alignment rates. In contrast, BWA-MEM, which offers greater tolerance for indels, repeats, and sequencing errors, exhibited substantially improved alignment performance, consistent with previous findings in complex genomes (Wu et al., 2019). Implementation of BWA-MEM increased mapping rates from approximately 50% to over 90% (Supplementary Table S2). Additionally, to address issues of multi-mapping in repeat-rich genomes, a common feature among marine invertebrates (Fallet et al., 2020), paired-end 150 bp (PE150) sequencing was employed to ensure sufficient read lengths for capturing 180 bp CUT&Tag fragments corresponding to single nucleosome-sized DNA.

CUT&Tag performance was validated by assessing alignment rates and fragment profiles. Most samples exhibited alignment rates exceeding 90%, with all samples achieving rates above 70%, indicating high mapping efficiency (Supplementary Table S2). Fragment size distribution revealed clear nucleosomal laddering in most histone-marked samples, whereas IgG controls lacked such patterns (Figure 1A; Supplementary Figure S1A), confirming specific enrichment of histone modifications (Brahma & Henikoff, 2024; Ye et al., 2021). At the zygote stage, both mononucleosome and subnucleosomal fragments were detected, whereas no mononucleosome-sized fragments were observed at the 4-cell stage (Supplementary Figure S1A), potentially reflecting dynamic nucleosome reorganization during rapid cell divisions in early embryogenesis (Pecori &

Torres-Padilla, 2023; Wang et al., 2022).

Correlation analysis demonstrated moderate to high reproducibility across biological replicates. Moreover, the activating histone marks (H3K27ac, H3K4me1, and H3K4me3) exhibited stronger correlations among themselves than with either the IgG controls or repressive mark H3K27me3 (Figure 1B), supporting the specificity and consistency of the CUT&Tag profiles. These results are consistent with previous findings, particularly considering the higher cellular heterogeneity present in whole-embryo samples used in this study (Ye et al., 2021). Signal enrichment analysis revealed strong peak-centered signals for all four histone marks, while IgG controls exhibited no enrichment (Figure 1C), further validating peak specificity and reliability (Kaya-Okur et al., 2019).

Genome-wide distribution analysis revealed histone mark patterns consistent with those reported in other species (Boileau et al., 2023; Crespo et al., 2020; Pekowska et al., 2011; Pinello et al., 2014) (Supplementary Figure S1B). H3K4me3 was significantly enriched around TSS (Figure 1D), consistent with its canonical association with active promoters (Millán-Zambrano et al., 2022). Histone marks exhibited differential enrichment across genomic regions. At the trochophore stage, promoter-associated peaks accounted for 38% (H3K4me1), 52% (H3K4me3), 28% (H3K27me3), and 32% (H3K27ac), while peaks in distal intergenic regions accounted for 54%, 40%, 57%, and 48%, respectively. Peaks in untranslated regions (UTRs), exons, introns, and downstream regions contained comparatively fewer peaks (Figure 1E, F; Supplementary Figure S1B). These patterns indicate predominant localization of histone modifications in promoters and distal intergenic regions, highlighting their key regulatory roles. Notably, H3K27me3 remained stably distributed across genomic regions over the 6 developmental stages, while H3K4me1, H3K4me3, and H3K27ac exhibited pronounced redistribution between the morula and gastrula stages (Figure S1B), suggesting major chromatin remodeling and transcriptional activation events during this developmental window (Bae & Lesch, 2020; Yu et al., 2023).

Collectively, these results confirm the successful establishment and adaptation of CUT&Tag for *M. lateralis*, enabling robust profiling of histone modifications throughout embryogenesis. Given the conserved cellular and genomic features among marine invertebrates, this optimized protocol is likely to be broadly applicable across related taxa.

Chromatin state profiling during early embryogenesis in *M. lateralis*

Transcriptional regulation during embryonic development involves dynamic shifts in chromatin states that interact with trans-acting factors such as transcription factors. These chromatin states, defined by combinations of epigenetic modifications, not only reflect temporal changes in genome accessibility but also enable annotation of regulatory element and functional genomic regions across developmental stages (Ernst & Kellis, 2017; Liu et al., 2024). While individual histone marks provide valuable information about chromatin accessibility and transcriptional regulation, analyzing combinatorial patterns of multiple histone marks allows for a more comprehensive classification of chromatin states. These states correspond to distinct functional genomic elements, including promoters, enhancers, actively transcribed regions, and repressed domains, serving as a foundation for annotating functional elements in the *M. lateralis* genome.

To systematically define chromatin states in *M. lateralis*, ChromHMM, a computational tool for epigenomic annotation (Ernst & Kellis, 2017), was applied to genome-wide CUT&Tag profiles of four histone modifications—H3K4me1, H3K4me3, H3K27me3, and H3K27ac. Although chromatin state analyses are well established in vertebrate models, including mammals and fish, such approaches remain limited in bivalves (Fukushima et al., 2023; Rivera-Casas et al., 2017; Sotomayor-Lugo et al., 2024; Zhu et al., 2019). To address this gap, chromatin state modeling was conducted in *M. lateralis* embryos to resolve the epigenomic landscape underlying early development.

Ten distinct chromatin states were inferred based on integration of the four histone modification marks, following standard ChromHMM protocols (Ernst & Kellis, 2017). These states were functionally interpreted based on histone mark combinations and genomic localization patterns (Ernst & Kellis, 2017; Roadmap Epigenomics Consortium et al., 2015), including: Active TSS (TssA), Flanking TSS (TssFlnk), Active Enhancer (EnhA1), Active Enhancer (EnhA2), Flanking Bivalent TSS/Enh (BivFlnk), Weak Flanking Bivalent TSS/Enh (BivFlnkWK), Repressed Polycomb (ReprPC), Weak Repressed Polycomb (ReprPCWk), Weak Transcription (TxWk), and Quiescent/low (Quies). TssA and TssFlnk, located near TSS, were both enriched for H3K4me3, with TssA also marked by H3K4me1 and H3K27ac, indicative of transcriptionally active promoters. EnhA1 and EnhA2 were enriched for H3K27ac, with EnhA1 showing higher H3K4me1 levels, consistent with active enhancer activity. Bivalent states co-enriched for active and repressive marks (e.g., H3K4me3/H3K27me3) may represent poised regulatory regions. ReprPC and ReprPCWk were defined by H3K27me3 enrichment, indicating polycomb-mediated repression. TxWk and Quies represented weakly transcribed or modification-depleted regions, respectively. It is important to note that ChromHMM state labels are based on probabilistic mark combinations and do not represent definitive functional assignments. For example, H3K4me1 may occur at both promoters and enhancers, and transitions between states (e.g., EnhA→TssFlnk→EnhA) may reflect dynamic regulatory element reuse rather than fixed functions. Interpretation of chromatin states should consider histone mark intensities, emission probabilities (Figure 2A), genomic annotations (Figure 2B), and gene expression profiles. The full chromatin state model captures the spectrum of transcriptional, enhancer, bivalent, repressive, and quiescent chromatin patterns and provides a genome-wide regulatory annotation for *M. lateralis* (Figure 2A–C).

To assess the biological relevance of the predicted chromatin states, the gene *sec61a* (FF-mul00016189) was examined as a representative locus. This gene encodes a conserved component of the SEC61 translocon complex, which facilitates co-translational protein transport into the endoplasmic reticulum and is involved in intracellular signaling (Bolar et al., 2016; Linxweiler et al., 2017). *Sec61a* exhibited significant up-regulation during the gastrula and trochophore stages, with corresponding chromatin states including TssFlnk, TssFlnkU, and enhancer-associated signatures enriched for H3K4me1 and H3K27ac. Visualization in IGV and gene expression analysis confirmed strong activation coinciding with predicted regulatory states (Figure 2D–E), supporting the functional relevance of the chromatin state

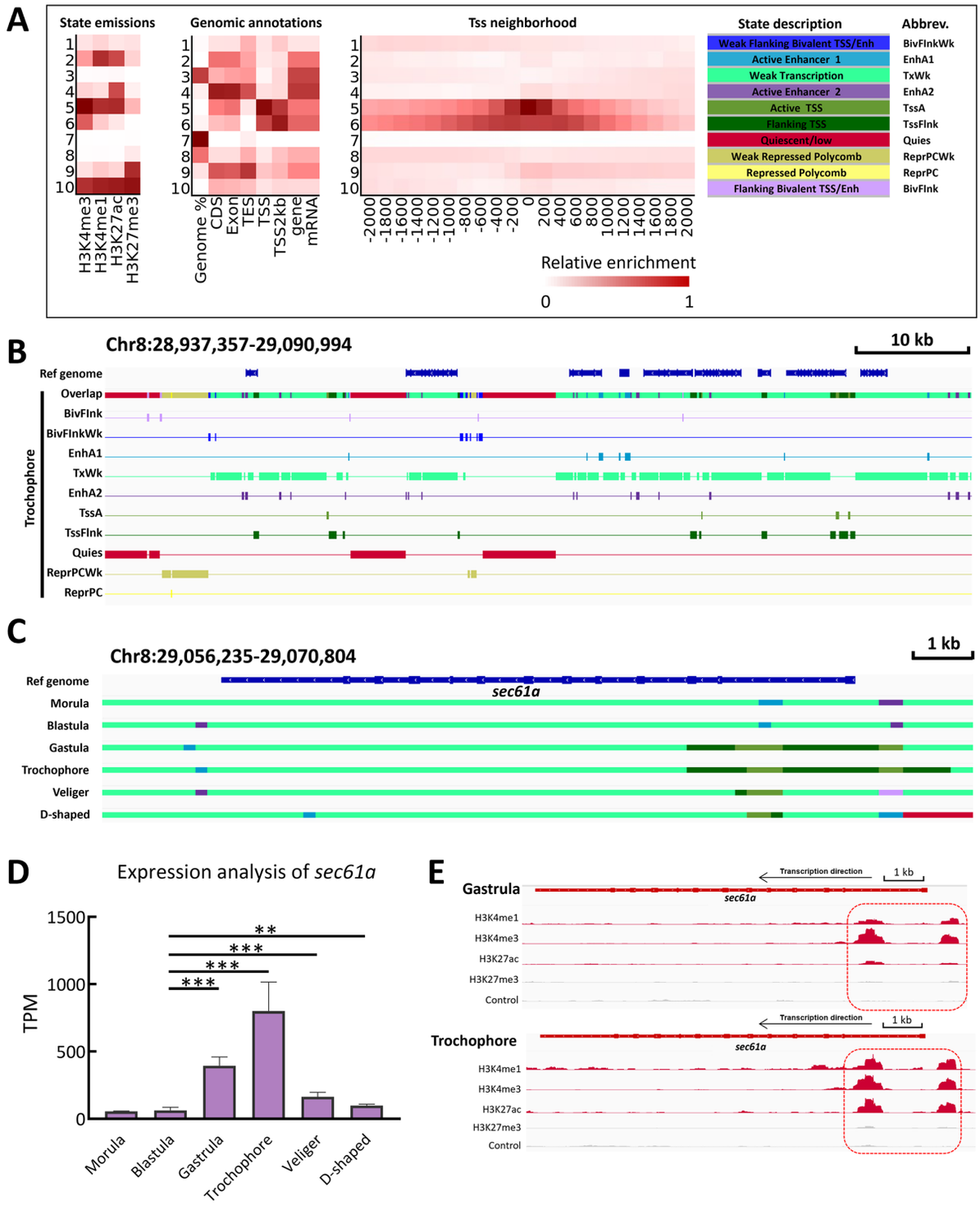

Figure 2 Chromatin state annotation using ChromHMM in *Mulinia lateralis* embryos

A: Chromatin states identified by chromHMM. Left panel: Heatmap of 10-state model emission parameters, with rows representing distinct chromatin states and columns representing histone marks. Color intensity represents probability of a given mark occurring in a particular state. Middle panel: Heatmap depicting enrichment of chromatin states at external genomic annotations, with color gradient reflecting degree of enrichment. Right panel: Heatmap illustrating enrichment of chromatin states within ±2 kb of TSS, with darker red indicating stronger enrichment and one color scale used for the entire heatmap. Candidate-state descriptions with abbreviations are listed on the right. B: Genome browser view of chromatin states (cis-regulatory elements) identified by ChromHMM. Chromatin state tracks for trochophore stage are shown, with chromatin states displayed either in a compact format (all states combined) or individually (per state). C: Genome browser view of ChromHMM-based chromatin state annotations at the *sec61a* (FF-mul00016189) locus across six developmental stages of *M. lateralis* embryos. Each row represents a specific stage, and chromatin state colors are consistent across all panels. D: Expression levels of *sec61a* during *M. lateralis* embryonic development, quantified in transcripts per million (TPM). **: P<0.01; ***: P<0.001. E: IGV genome browser view displaying histone modification signal enrichment at the *sec61a* locus during the gastrula and trochophore stages, demonstrating correct chromatin state assignments as shown in C and confirming their association with transcriptional activity in D.

annotations. This chromatin state atlas provides a crucial reference for the functional genome annotation in *M. lateralis*. Integration with transcriptomic and epigenomic data offers insights into regulatory dynamics during embryogenesis and establishes a platform for comparative epigenomic analyses across marine invertebrates, contributing to a broader understanding of chromatin-mediated gene regulation in bivalves and evolutionary and developmental epigenomics. The complete chromatin state annotation dataset is available in the Supplementary File.

Histone modification dynamics and chromatin remodeling during early embryogenesis in *M. lateralis*

To elucidate histone modification dynamics during early embryonic development, genome-wide profiling of the four histone modifications was performed. Analysis of peak counts and the proportion of associated genes relative to the total annotated gene set revealed low abundance during early stages, followed by a substantial increase at the gastrula stage (Figure 3A). A corresponding rise in the proportion of genes associated with these marks was observed (Figure 3B), suggesting that histone modification remodeling occurs evenly across the genome rather than confined to specific loci. Among the four marks, H3K27me3 exhibited the earliest and broadest genomic distribution, with over 5 000 peaks corresponding to 14.65% of annotated genes at the morula stage (Figure 3A, B). This early enrichment of a repressive modification suggests the establishment of chromatin-based silencing before widespread ZGA, potentially restraining premature activation of developmental genes prior to lineage commitment (Lindeman et al., 2011; Xia et al., 2019). In contrast, permissive histone modifications such as H3K4me3, H3K4me1, and H3K27ac accumulated more gradually and reached wide prevalence at the gastrula stage (Figure 3A, B).

Given that deposition of H3K27me3 is catalyzed by PRC2 (Millán-Zambrano et al., 2022; Xia et al., 2019), transcript levels of its core components (EZH2, SUZ12, and EED) were examined to assess PRC2 activity during early chromatin regulation. Transcriptomic analysis revealed that *ezh2* (FF-mul00015448), encoding the PRC2 catalytic subunit, was highly expressed at the morula and blastula stages (Supplementary Figure S2A), supporting its role in early chromatin remodeling. Similarly, elevated transcript levels of *eed* (FF-mul00005678) and *suz12* (FF-mul00001742) at the morula stage (Supplementary Figure S2B, C) further support the functional activity of PRC2 during this period. The temporal correlation between increased PRC2 component expression and H3K27me3 accumulation further supports the potential role of PRC2 in mediating early chromatin repression at specific sites before widespread ZGA. Comparable mechanisms have been observed in zebrafish and mammals, where PRC2 activity is critical for suppressing premature gene activation (Lindeman et al., 2011; Xia et al., 2019). Among these components, *EZH2* was identified as a key regulatory factor through integrated CUT&Tag and RNA-seq analysis (detailed in Section 3.6), which revealed its active zygotic transcription during the blastula stage (Figure 3C). To further examine its evolutionary conservation, phylogenetic and domain analyses were performed. In metazoans, two *EZH* genes—*EZH1* and *EZH2*—originated from a duplication event in a common ancestor of cartilaginous fish and bony vertebrates (Völkel et al., 2019). Unlike vertebrates, which possess both *EZH1* and *EZH2*, invertebrates possess only *EZH2* (Völkel et al., 2019). Consistent with this pattern, only a single *ezh2* gene was detected in the *M. lateralis* genome. Phylogenetic analysis positioned *M. lateralis* EZH2 within the molluscan clade, showing close evolutionary proximity to arthropod homologs and distinct separation from vertebrate EZH2 sequences (Supplementary Figure S2D). The domain structure of EZH2 in *M. lateralis* included conserved SANT, CXC, and SET domains, characteristic of functional histone methyltransferases (HMTases) (Supplementary Figure S2E). The SET domain, located at the C-terminus, contains the catalytic subunit responsible for H3K27 methylation (Sun et al., 2023). Comparative analysis of the SET domain revealed the substitution of amino acid residues Ile34 and Cys52 by Leu34 and Ser52 in EZH1 (Supplementary Figure S2F). These findings support the hypothesis that early repressive chromatin regulation in *M. lateralis* shares key evolutionary features with other metazoans but may also exhibit lineage-specific adaptations in bivalves. Future studies exploring PRC2-associated cofactors and regulatory mechanisms in mollusks may provide further insights into the evolutionary divergence of histone methylation pathways across invertebrates.

To provide ultrastructural validation of chromatin reorganization during early development, TEM was performed at key developmental stages (Laue et al., 2019). Consistent with histone modification profiles, dense chromatin aggregates were observed in nuclei at the blastula-stage and beyond, while such structures were sparse or absent during earlier stages (Figure 3D–G). These results suggest progressive compaction during development, aligning with the observed increase in repressive histone modification levels. Quantitative analyses of histone modification signal intensity and peak enrichment further supported this transition from an initially relaxed chromatin state to a more structured and repressed configuration (Figure 3H; Supplementary Figure S3A–D). The TEM results thus provide strong structural evidence for extensive chromatin remodeling during early embryogenesis.

The onset of widespread ZGA between the gastrula and trochophore stages was accompanied by a marked increase in permissive histone modifications, particularly H3K4me1, H3K4me3, and H3K27ac, consistent with their roles in enhancer and promoter activation (Millán-Zambrano et al., 2022). Transcriptomic profiling showed that *setd1b* (FF-mul00014078), one of the HMTases responsible for catalyzing H3K4 methylation and essential for embryogenesis and organogenesis—particularly during post-gastrula development (Kranz & Anastassiadis, 2020)—exhibited relatively stable mRNA levels throughout embryogenesis, while *wdr5* (FF-mul00021417) and *rbbp5* (FF-mul00018773), core scaffolding components of the H3K4 methyltransferase complex that facilitate catalytic activity (Hanna et al., 2022), showed increased expression from the gastrula stage (Supplementary Figure S3E–G). These findings suggest that the deposition of H3K4 methylation may be closely linked to the activation of zygotic transcription.

Dynamic transcriptomic and epigenetic reprogramming during MZT in *M. lateralis*

PCA of the transcriptomic data confirmed high reproducibility among biological replicates (Supplementary Figure S4A). Interestingly, samples from the eight developmental stages clustered into three distinct groups, indicating distinct transcriptional shifts. The blastula and gastrula stages formed

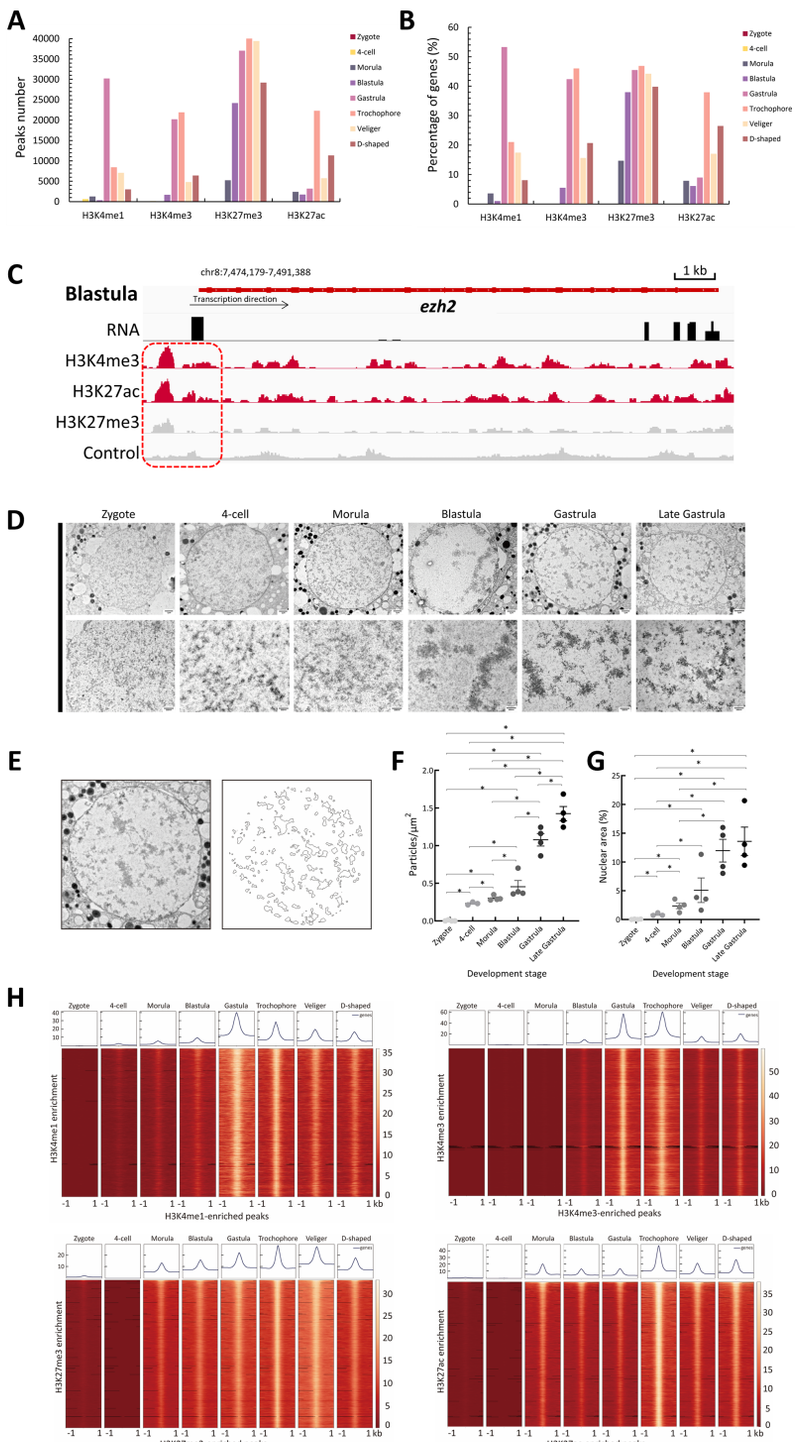

Figure 3 Histone modification dynamics during early embryonic development in *Mulinia lateralis*

A: Number of enriched peaks for H3K4me1, H3K4me3, H3K27me3, and H3K27ac across eight key developmental stages, illustrating dynamic chromatin landscape. B: Proportion of genes marked by each histone modification relative to the total number of genes in the genome at different developmental stages, reflecting progressive chromatin remodeling and transcriptional regulation. C: IGV view of *ezh2* expression and histone modification patterns at genomic loci during the blastula stage. Promoter region exhibits co-occurring H3K4me3 and H3K27ac peaks, indicative of active transcription, whereas H3K27me3 remains weakly enriched. D: Transmission electron micrographs of chromatin ultrastructure in embryonic cell nuclei at different developmental stages. Higher magnification images highlight chromatin organization. Scale bars: 1 μm (nuclear images), 500 nm (high-magnification insets). E: Representative image illustrating electron-dense particle detection. F: Quantification of the number of particles per nuclear μm^2 in TEM images from zygote to late gastrula stage. G: Quantification of nuclear area (%) covered by particles in TEM images from the zygote to late gastrula stages. Nuclei from 3–4 embryos were analyzed per time point for electron-dense aggregate quantification. Each point represents data from one nucleus. *P*-values were calculated using Kruskal-Wallis tests (*: P<0.05), with error bars indicating standard deviation (SD). H: Heatmap of histone modification signal enrichment at all identified peak regions across eight key developmental stages. Signal intensities for H3K4me1, H3K4me3, H3K27me3, and H3K27ac are centered on peak summits and plotted within ±1 000 bp regions.

one cluster, while trochophore, veliger, and D-shaped larvae grouped together. In contrast, the zygote, 4-cell, and morula stages exhibited the most distinct gene expression patterns, likely reflecting the dominance of maternal mRNA during early development (Vastenhouw et al., 2019). Sample correlation analysis also demonstrated strong within-stage concordance among biological replicates, particularly among the early stages (Supplementary Figure S4B), further validating the stability and reproducibility of the data. Transcriptome profiling revealed that approximately 70% of annotated genes were expressed between the zygote and morula stages, consistent with patterns observed in *Drosophila melanogaster*, *Strongylocentrotus purpuratus*, and zebrafish (Vastenhouw et al., 2019). A sharp decline in RNA levels occurred at the blastula stage, suggesting large-scale maternal mRNA degradation between the morula and blastula stages. From the gastrula stage onward, gene detection gradually recovered and stabilized by the trochophore stage (Supplementary Figure S4C), indicating successful establishment of ZGA.

Maternal mRNA degradation may involve processing body (P-body)-mediated decay, as evidenced by the elevated expression of key P-body-associated genes *lsm14a* (FF-mul00010230) and *pdap1* (FF-mul00001599) during the blastula stage (Supplementary Figure S4D, E). LSM14A facilitates P-body formation and plays a major role in mRNA decay and storage (Brandmann et al., 2018; Stefano et al., 2019). PDAP1, a highly conserved P-body component, modulates *limd1* expression and contributes to P-body stability (Chirichella et al., 2022). Given that P-bodies function as hubs for post-translational regulation, the observed expression profiles suggest their involvement in maternal mRNA clearance during early embryogenesis (Beadle et al., 2023). However, direct evidence linking P-body activity to global maternal transcript degradation in *M. lateralis* remains to be established.

Histone modifications were also dynamically reprogrammed during embryogenesis, indicating coordinated epigenetic regulation of the MZT in *M. lateralis*. In the earliest stages (zygote to 4-cell), histone modifications were nearly undetectable, except for a few H3K4me1-marked loci (Figure 3A, B), and chromatin remained in a relatively relaxed state (Figure 3D). This transcriptionally permissive state supported maternal mRNA-driven development. By the morula stage, repressive histone mark H3K27me3 was already widespread, while permissive marks (H3K4me1 and H3K27ac) appeared at low abundance (Figure 3A, B). Early enrichment of the repressive mark likely contributed to transcriptional regression by preventing premature gene activation at selected sites. Concurrently, maternal mRNA degradation had commenced. During the blastula stage, maternal mRNA degradation peaked, RNA levels declined, and permissive H3K4me3 began to accumulate (Figures 3A, B, 5A; Supplementary Figure S4C), suggesting tight control of transcriptional activation. By the gastrula stage, ZGA was fully established, with widespread histone modifications, increased chromatin compaction, and transcriptional up-regulation (Figure 3A, B). These changes aligned with significant cellular differentiation events, suggesting that histone modifications may facilitate precise gene regulatory mechanisms during *M. lateralis* embryogenesis.

Collectively, these findings indicate that the MZT in *M. lateralis* occurs predominantly between the morula and gastrula stages, characterized by synchronized maternal mRNA transcript clearance and zygotic transcriptional activation (Figure 4). The coordinated regulation of histone modifications and transcriptional reprogramming provides a comprehensive molecular framework for understanding early embryonic regulation in bivalves and lay a foundation for future research into epigenetic regulation in marine invertebrate development.

Stage-specific gene expression dynamics and co-expression network architecture during *M. lateralis* embryogenesis

Integration of chromatin and transcriptomic profiling identified the MZT in *M. lateralis* as occurring between the morula and gastrula stages (Figure 4). To further resolve stage-specific transcriptional programs associated with zygotic genome activation, differential gene expression analysis was performed between consecutive developmental stages starting at the morula. KEGG enrichment analysis was subsequently applied to interpret functional associations of the identified DEGs. Marked transcriptomic reprogramming was observed, with significant up-regulation and down-regulation of mRNA levels across all stage transitions. Notably, the largest number of DEGs was detected between the blastula and morula stages, with 924 genes up-regulated and 5 029 genes down-regulated, consistent with widespread maternal mRNA degradation during this period. The observed increase in mRNA abundance at the blastula stage may, in part, reflect cytoplasmic polyadenylation of maternal mRNAs, a widely conserved mechanism across animal species during early embryogenesis (Subtelny et al., 2014). As embryonic development progressed, transcriptomic changes became more stage-specific, with 86, 384, 218, and 696 genes up-regulated at the gastrula, trochophore, veliger, and D-shaped larval stages, respectively (Figure 5A). These findings indicate a progressive establishment of zygotic transcriptional programs orchestrating stage-specific developmental processes in *M. lateralis*.

KEGG pathway enrichment analysis revealed dynamic functional reprogramming throughout development. During the blastula stage, DEGs were enriched in pathways associated with ribosome biogenesis, nucleocytoplasmic transport, and ErbB signaling, supporting rapid cell proliferation and division (Figure 5B). At the gastrula stage, DEGs were enriched in AMPK signaling and pluripotency-associated regulation, reflecting cell differentiation and germ layer formation. The trochophore and veliger stages were characterized by the up-regulation of genes involved in muscle development, immune response, and nervous system formation, including actin cytoskeleton regulation, leukocyte transendothelial migration, and Hippo signaling. By the D-shaped larval stage, genes related to energy metabolism and lipid biosynthesis pathways, such as cortisol synthesis and secretion, steroid hormone biosynthesis, and adipocytokine signaling, were up-regulated, corresponding to shell formation and larval development (Figure 5B). However, it is important to note that during early stages, particularly the blastula stage, functional analysis of DEGs based on RNA-seq data should be interpreted with caution due to the substantial influence of maternal RNAs.

To delineate transcriptional modules underlying coordinated gene expression, WGCNA was performed, grouping genes into eight co-expression modules (M1–M8) with distinct temporal expression patterns (Figure 6A, B). Each module exhibited stage-specific activation and enrichment in

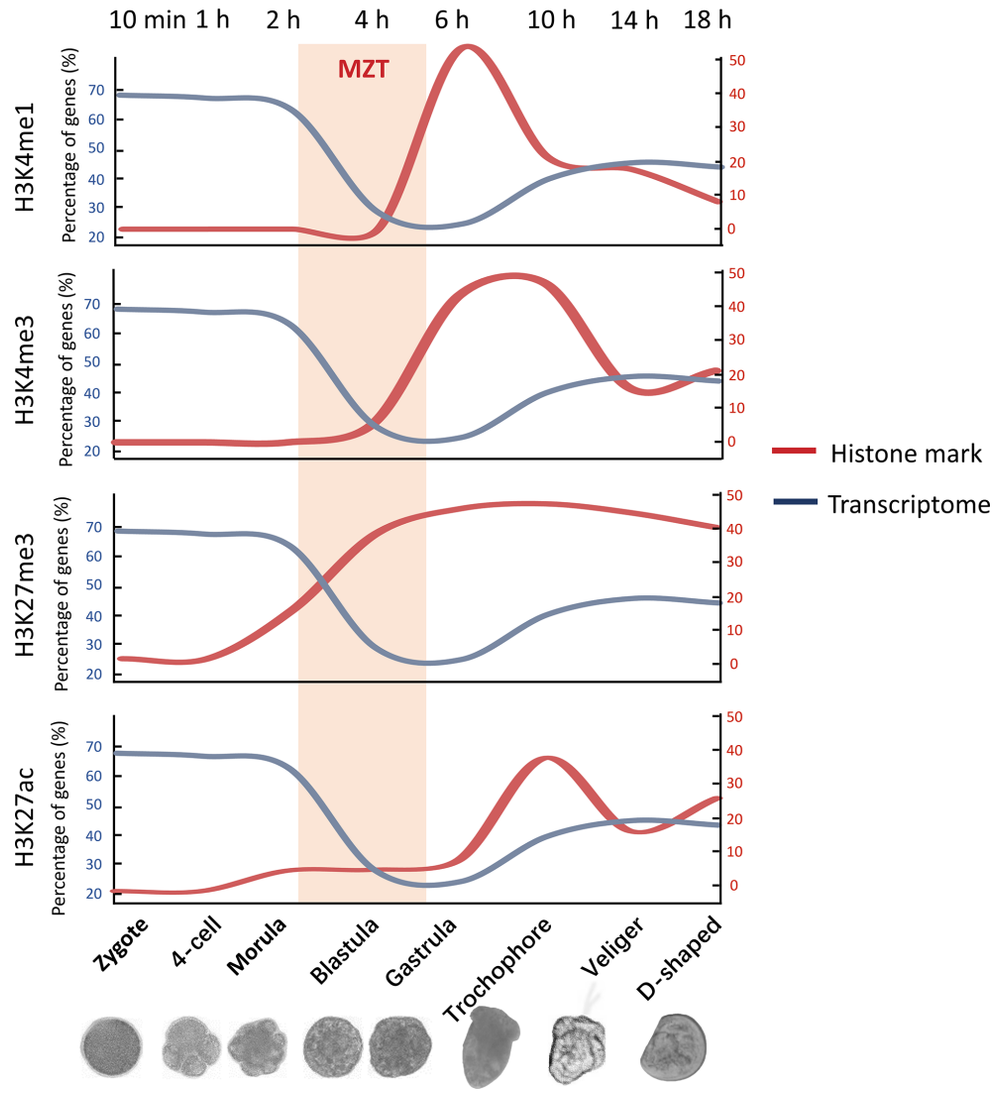

Figure 4 Dynamic model of histone modification changes and transcriptional activity during early embryonic development in *Mulinia lateralis*

Red curves represent temporal dynamics of histone modifications (left y-axis: percentage of genes with histone modifications), while blue curves illustrate transcriptional activity levels (right y-axis: percentage of expressed genes). Each developmental stage is accompanied by a corresponding embryo schematic below, depicting key morphological transitions. Results indicate that as the MZT progresses, maternal mRNA clearance and zygotic genome activation predominantly occur between the morula and gastrula stages, likely driven by the coordinated regulation of histone modifications and transcriptional dynamics.

biologically relevant pathways (Figure 6C). The M3 module, highly expressed at the blastula stage, was enriched in Hippo signaling, a pathway central to cell proliferation and apoptosis (Meléndez García et al., 2022). Modules M4 and M5, predominantly expressed at the gastrula stage, were enriched in TGF-β signaling, a key regulator of gastrulation and embryonic patterning (Zinski et al., 2018). The M6 module, active during the trochophore stage, was enriched in MAPK signaling, supporting cell proliferation, differentiation, and metabolism (Zhang & Liu, 2002). The M1 and M2 modules, expressed during the D-shaped stage, were enriched in metabolic and transport-related pathways, reflecting increased metabolic demand and active biomineralization processes (Guo et al., 2023).

Overall, the DEG and WGCNA results were highly consistent, revealing stage-specific transcriptional regulation and key pathways underlying *M. lateralis* embryogenesis. Differential analysis identified developmentally critical pathways, from cell proliferation in the blastula stage to biomineralization in D-shaped larva, while WGCNA provided insights into co-regulated gene networks driving these processes. These findings suggest that key signaling pathways, particularly Hippo, TGF-β, and MAPK, play essential roles in *M. lateralis* embryogenesis and larval development, providing a comprehensive framework for understanding the molecular mechanisms regulating early development in bivalves.

Identification of actively transcribing genes during *M. lateralis* embryogenesis via integrative chromatin and transcriptomic analysis

Histone modifications provide real-time indicators of chromatin accessibility and transcriptional potential, whereas RNA-seq captures accumulated transcript levels, reflecting the combined outcome of transcription and mRNA decay. Precise activation of zygotic genes is essential for proper embryonic progression (Bannister & Kouzarides, 2011; Schulz &

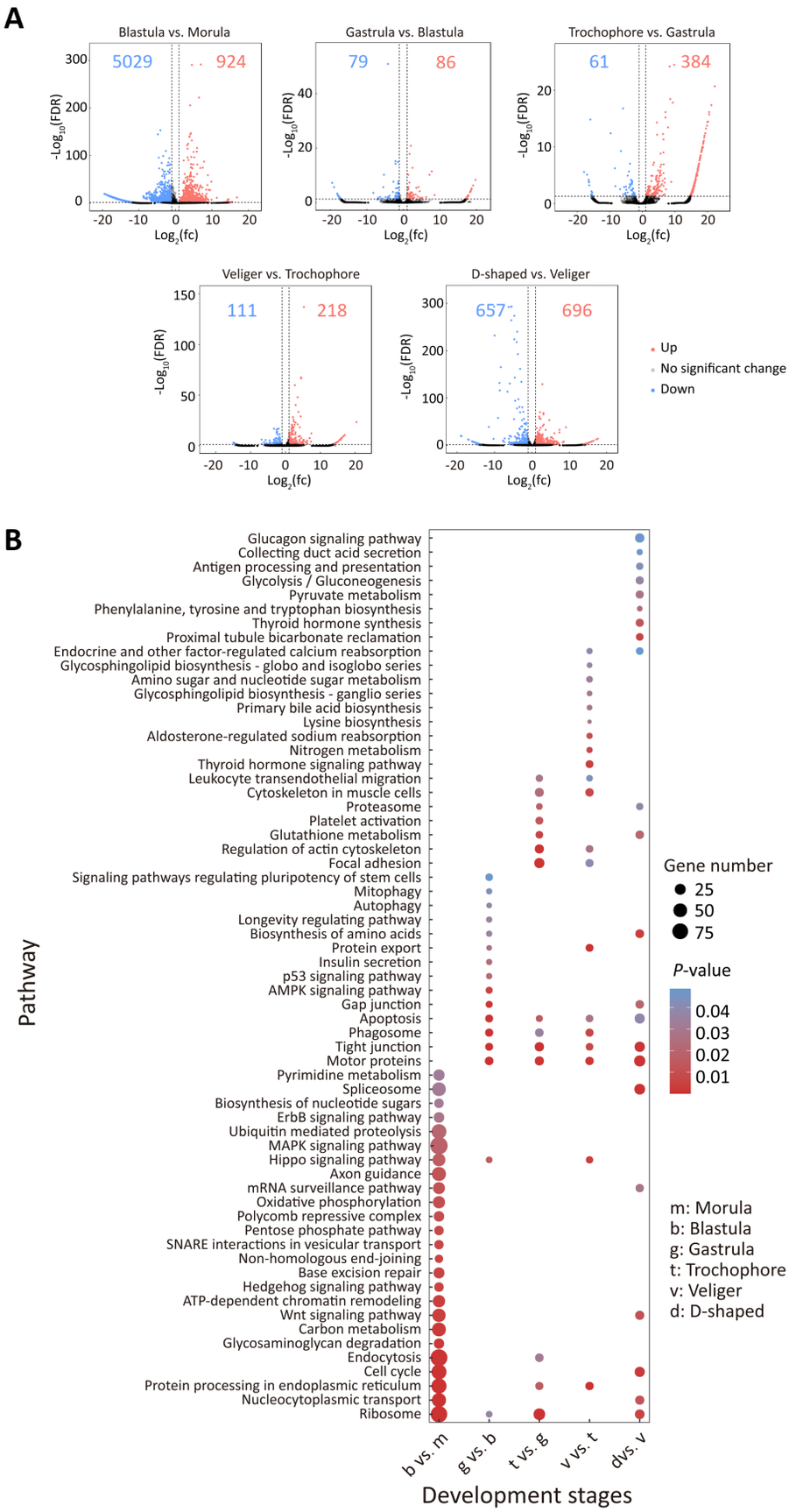

Figure 5 Differential expression analysis during *Mulinia lateralis* embryonic development

A: Volcano plot visualization of differentially expressed genes (DEGs). Significantly up-regulated ("Up") and down-regulated ("Down") genes are numerically annotated, with displayed counts indicating magnitude of transcriptional changes between comparative groups, illustrating major transcriptional transitions. B: KEGG pathway enrichment analysis of DEGs at each developmental stage, visualized as a bubble chart. Size of each bubble reflects gene count, and color scale represents statistical significance of enrichment.

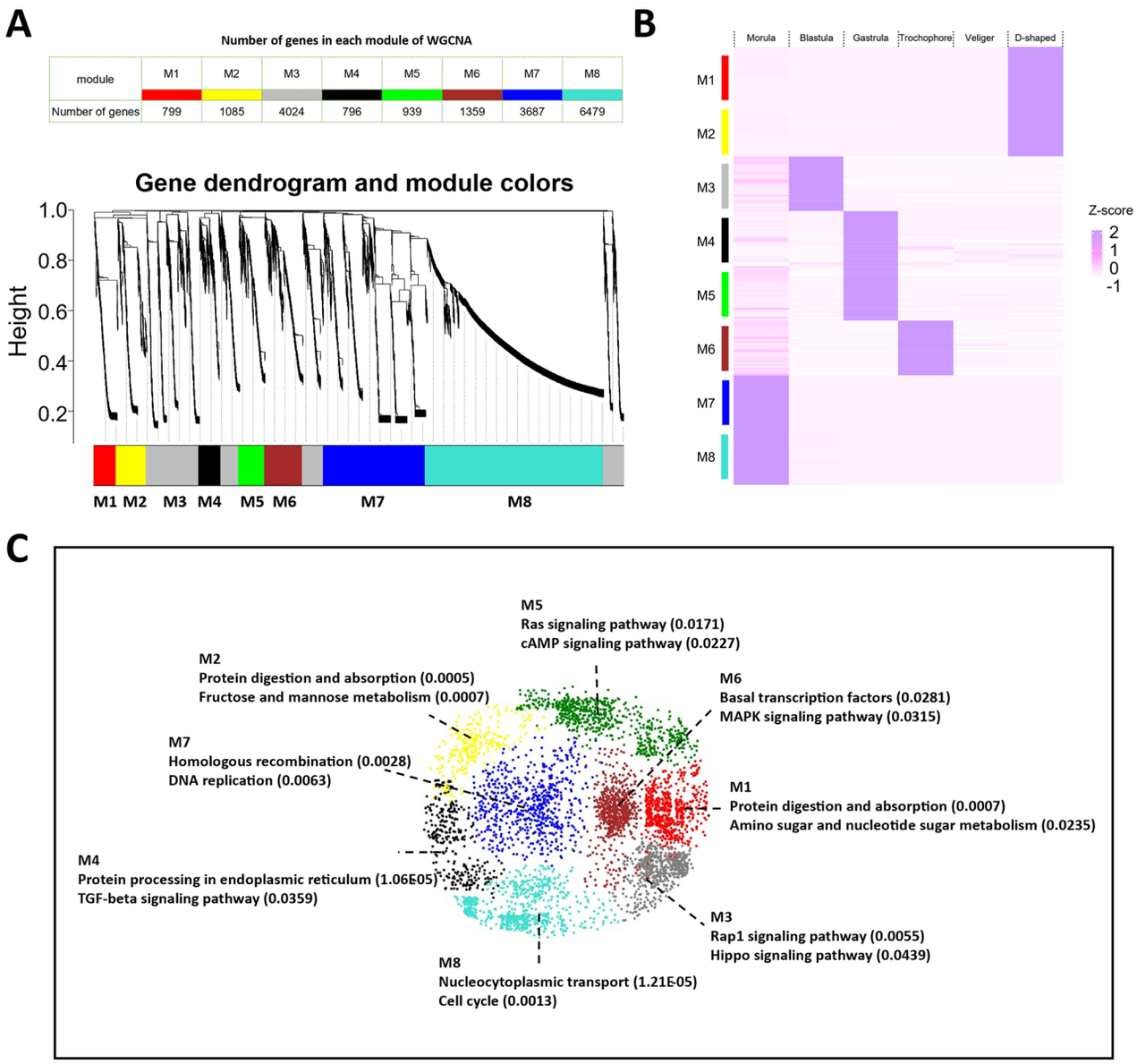

Figure 6 Weighted gene co-expression network analysis (WGCNA) of embryonic development in *Mulinia lateralis*

A: WGCNA identified eight gene expression modules across six embryonic stages, providing insight into stage-specific regulatory networks. B: Heatmap of the top 30 most highly connected genes within each WGCNA module, showing stage-specific expression patterns. C: Co-expression network and KEGG enrichment analysis of WGCNA modules. Only the two most significantly enriched pathways for each module are displayed. Numbers in parentheses indicate pathway-specific *P*-values.

Harrison, 2019; Turner, 2007). Genes that are actively transcribed during specific stages often play crucial roles in shaping the developmental characteristics of that period. To systematically identify transcriptionally active genes during *M. lateralis* embryogenesis, CUT&Tag and RNA-seq data were integrated. Actively transcribed genes were defined as those with an average TPM≥1, enrichment of H3K4me3 and H3K27ac at the promoter, and no overlapping H3K27me3 signal. Based on these criteria, 11 actively transcribed genes were detected at the blastula stage, 444 at the gastrula stage, 2 077 at the trochophore stage, 163 at the veliger stage, and 372 at the D-shaped larval stage (Figure 7A).

Across all stages, 40.7%–70.6% of genes marked with promoter-localized H3K4me3 and H3K27ac without H3K27me3 exhibited TPM values ≥1, supporting the predictive value of these histone marks for transcriptional activity during development.

To investigate the biological relevance of these actively transcribing genes, KEGG pathway enrichment analysis was conducted. Results revealed significant enrichment in pathways related to organismal systems, environmental information processing, cellular processes, metabolism, and genetic information processing. Specifically, genes involved in signal transduction, transcription, translation, metabolism, nervous system development, and immune system regulation were highly represented (Figure 7B). These patterns were consistent with enrichment results from WGCNA and DEG analyses, reinforcing the functional significance of histone modifications in developmental gene regulation.

At the blastula stage, *yap1* (FF-mul00019389), a core effector of Hippo signaling, was identified as a key transcriptionally active gene (Figure 7B). Expression peaked at the blastula stage (Figure 8A, B), consistent with its role in promoting cell proliferation and dedifferentiation, processes

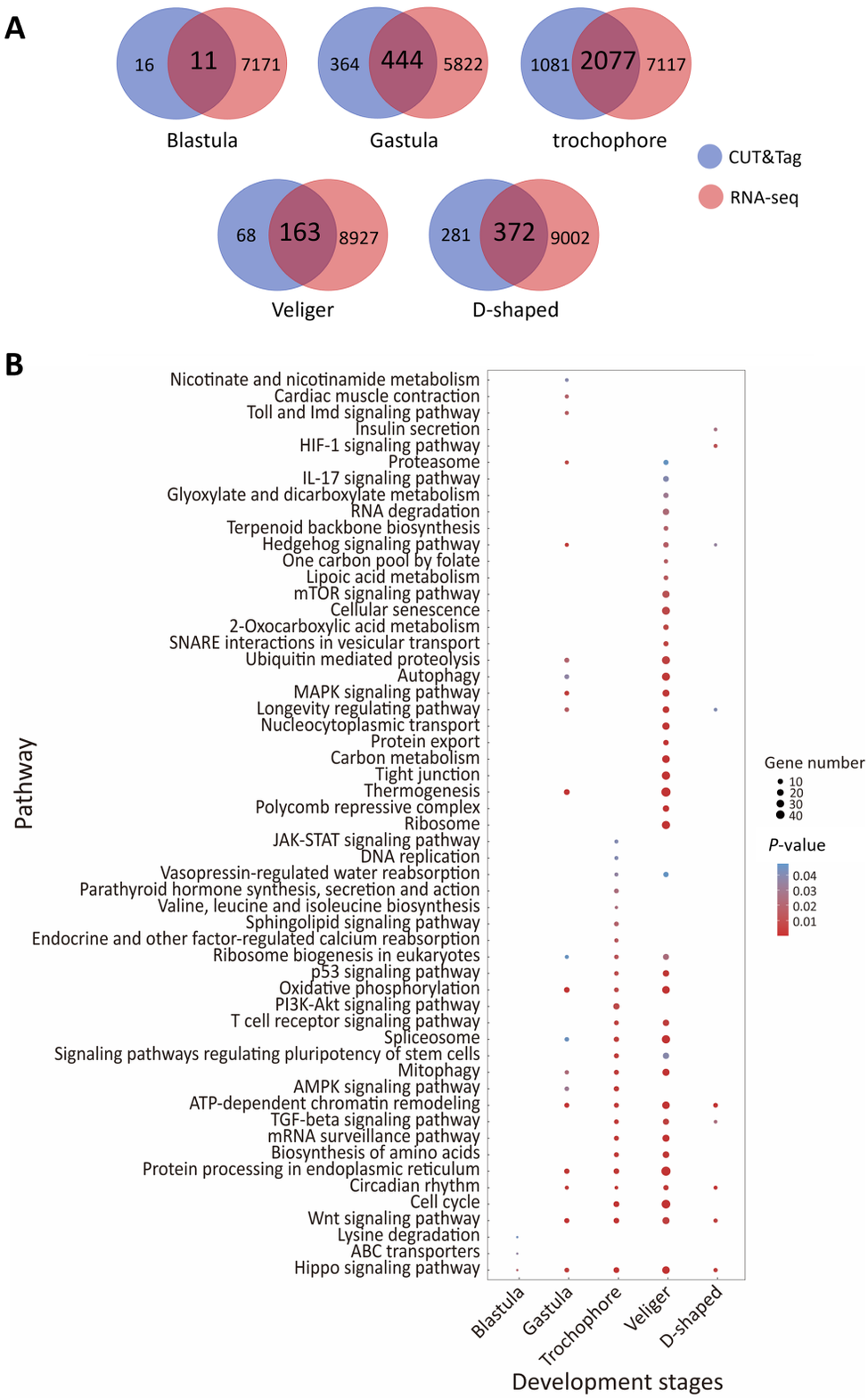

Figure 7 Identification of actively transcribing genes at each developmental stage through integrated CUT&Tag and transcriptome analysis and functional enrichment assessment

A: Number of actively transcribing genes identified at each developmental stage. Actively transcribing genes were defined as those with an average TPM≥1, promoter-enriched H3K4me3 and H3K27ac modifications, and an absence of H3K27me3 repression. Pink region in the Venn diagram represents the number of genes with a TPM≥1, while the green region represents genes identified via CUT&Tag (H3K4me3 peaks at the promoter region overlapping with H3K27ac peaks but not with H3K27me3 peaks). The intersection of these sets represents actively transcribing genes epigenetically marked by active histone modifications. B: KEGG pathway enrichment analysis of histone-marked, actively transcribing genes. Significantly enriched pathways (P<0.05) are visualized using a bubble plot, where bubble size indicates gene count and color intensity reflects statistical significance.

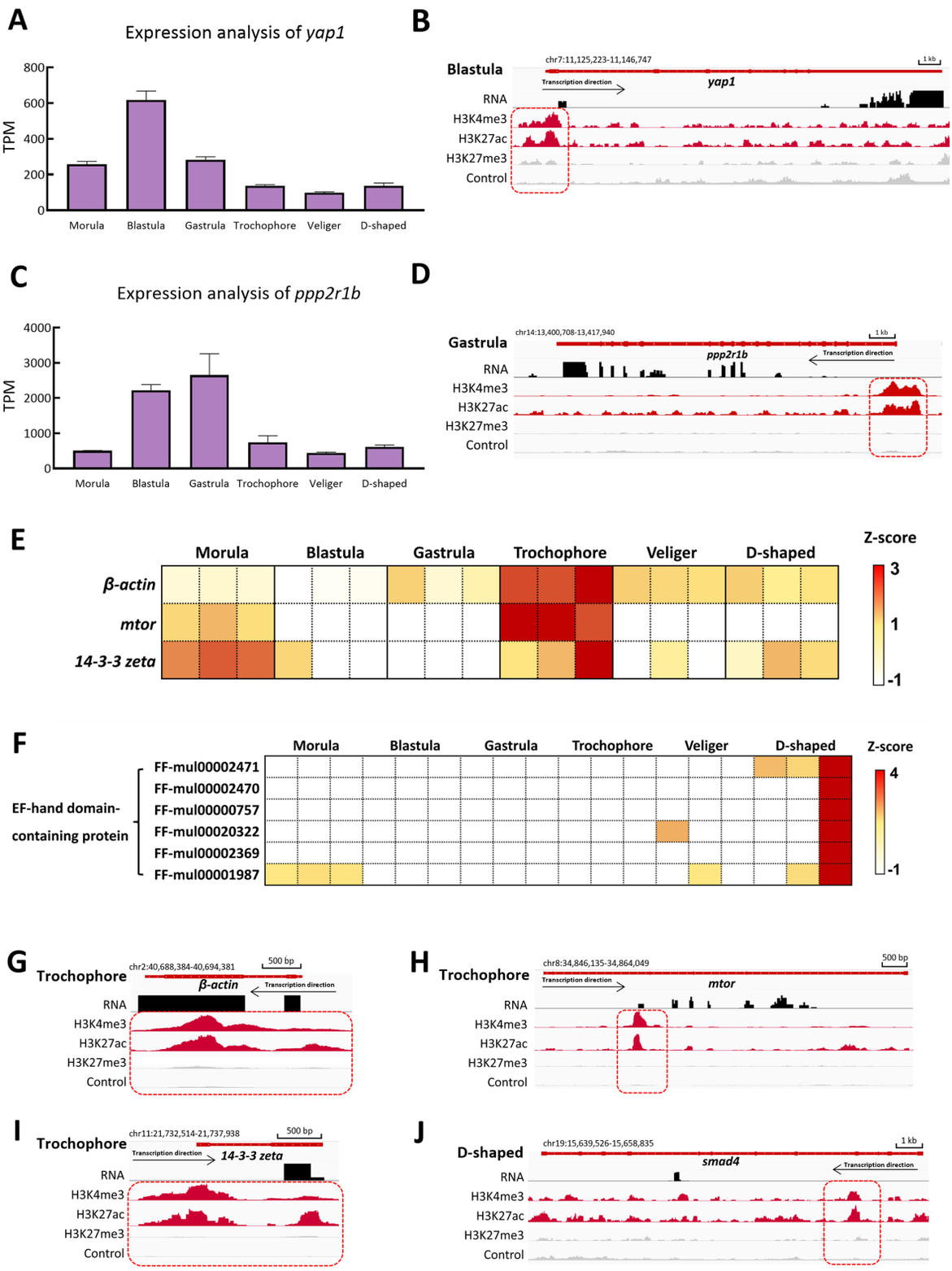

Figure 8 Examination of representative key actively transcribing genes identified through integrated analysis of histone modification and transcriptome data

B, D, G–J: IGV genome browser views displaying gene expression and histone modification enrichment patterns for key developmental regulators: *yap1* at the blastula stage (B), *ppp2r1b* at the gastrula stage (D), *β-actin*, *mtor*, and *14-3-3 zeta* at the trochophore stage (G–I), and *smad4* at the D-shaped larval stage (J). In all cases, H3K4me3 and H3K27ac are enriched at promoter regions, coinciding with active transcription, while H3K27me3 is absent, consistent with active gene regulation. A, C, E, F: Histograms or heatmaps showing transcript levels of *yap1*, *ppp2r1b*, *β-actin*, *mtor*, *14-3-3 zeta*, and EF-hand domain-containing proteins across developmental stages. Stage-specific up-regulation of these genes aligns with key developmental processes, confirming the reliability of combining histone modification profiles and transcriptomic data for identifying regulatory genes driving *Mulinia lateralis* embryogenesis.

central to blastula formation (Meléndez García et al., 2022). At the gastrula stage, *ppp2r1b* (FF-mul00018171), a component of protein phosphatase 2A (PP2A), was highly expressed and enriched in the TGF-β signaling pathway (Figures 7B, 8C, D). PPP2R1B supports WNT signaling activation, which plays a pivotal role in cell fate determination and axis patterning during gastrulation (Seshacharyulu et al., 2013). During the trochophore and veliger stages, actively transcribing genes overlapped significantly with those identified by RNA-seq, particularly in MAPK signaling and immune system development pathways (Figure 7B). Among these genes, *β-actin* (FF-mul00005415), *14-3-3 zeta* (FF-mul00020758), and *mtor* (FF-mul00016374) exhibited increasing expression from the trochophore stage onward (Figure 8E, G–I). These genes play essential roles in cell growth, neural development, embryonic left-right axis formation, and immune system regulation (Shen et al., 2018; Toyo-oka et al., 2003; Weichhart et al., 2015). At the D-shaped larval stage, *smad4* (FF-mul00024557) was identified as a transcriptionally active gene involved in shell calcification (Figure 8J). *Smad4* has been implicated in biomineralization and shell formation of various species, including *Crassostrea gigas*, *Lingula anatina*, and *Pinctada fucata* (Liu et al., 2014; Zhao et al., 2016). Transcriptomic analysis further revealed significant up-regulation of several shell mineralization-related genes, including FF-mul00002471, FF-mul00002470, FF-mul00000757, FF-mul00020322, FF-mul00002369, and FF-mul00001987 (Figure 8F). All encode proteins containing EF-hand domains, which are calcium-binding motifs known to regulate shell mineralization (Guo et al., 2023). These findings suggest that histone modifications play a crucial role in the epigenetic regulation of biomineralization pathways during larval development.

Through the integration of chromatin-state profiling and transcriptomic data, this study identified key genes involved in stage-specific processes, such as proliferation, signaling pathway regulation, neural and immune system development, and biomineralization. The resulting dataset serves as a comprehensive genome-wide reference for the cis-regulatory architecture of *M. lateralis* embryogenesis and provides a foundational framework for future functional studies on epigenetic regulation in bivalves. By characterizing the epigenetic regulatory elements that shape embryonic gene expression, this work offers a valuable resource for understanding the molecular mechanisms underlying early development in marine invertebrates.

DISCUSSION

Histone modification dynamics during early embryogenesis and their association with ZGA have remained a central focus in developmental biology. Conventional protein-DNA interaction assays, such as ChIP-seq, are limited by their high cell input requirements and the interference of abundant yolk proteins in early embryos, which hampers chromatin profiling during cleavage stages (Zhu et al., 2019). CUT&Tag has emerged as a powerful alternative, enabling high-resolution mapping of histone modifications using minimal input material, thereby facilitating investigation of chromatin accessibility and transcriptional regulation during early development (Kaya-Okur et al., 2019, 2020). Although CUT&Tag has been applied to various model organisms, including mammals, fish, and marine species (Bartosovic et al., 2021; Wu et al., 2021; Yang et al., 2022; Zheng et al., 2024), its utility in marine bivalves has not previously been demonstrated.

In the present study, an optimized CUT&Tag protocol was established and adapted to the cellular and genomic characteristics of *M. lateralis*. A marked improvement in alignment efficiency was observed when using BWA-MEM instead of Bowtie2 for mapping CUT&Tag data. Although a detailed comparison of alignment algorithms is beyond the scope of this work, the superior performance of BWA-MEM in *M. lateralis* likely reflects its capacity to handle repetitive sequences and structural complexity, both of which are prominent features in marine invertebrate genomes. Prior benchmarking has shown that BWA-MEM generally outperforms Bowtie2 in accuracy and sensitivity for complex genomes (Banović Đeri et al., 2024; Li, 2013; Li & Durbin, 2009). The resulting CUT&Tag data exhibited clear nucleosomal clarity and strong enrichment profiles, confirming the high data quality.

Using this optimized pipeline, high-resolution histone modification landscapes were profiled across key embryonic stages, focusing on H3K4me3, H3K4me1, H3K27me3, and H3K27ac—modifications with established roles in transcriptional regulation (Bannister & Kouzarides, 2011; Millán-Zambrano et al., 2022; Schulz & Harrison, 2019). Chromatin state modeling enabled systematic classification of cis-regulatory elements, revealing dynamic shifts in promoter, enhancer, and repressive chromatin states during development. Despite the potential for cellular heterogeneity in whole-embryo samples to introduce variability, integrated analyses of CUT&Tag and RNA-seq data confirmed a strong correlation between predicted regulatory elements and gene expression patterns (Figures 7, 8). These findings provide a foundational genomic annotation resource for *M. lateralis* and establish a framework for comparative epigenomic studies across marine invertebrates. Future studies employing single-cell or spatially resolved epigenomic techniques will be essential to further refine the spatial and temporal resolution of chromatin landscapes (Lu et al., 2022).

ZGA marks the MZT, a pivotal phase of embryogenesis characterized by extensive chromatin reprogramming and dynamic histone modifications. In *M. lateralis*, histone modifications were either initially absent or present at minimal levels during early cleavage stages. A pronounced chromatin remodeling event occurred between the morula and gastrula stages, coinciding with maternal mRNA degradation and the onset of widespread transcription. Notably, the repressive mark H3K27me3, associated with polycomb-mediated silencing, was already enriched at the morula stage, preceding genome-wide transcriptional activation. At this stage, H3K27me3 spanned a broader genomic territory than the activating marks H3K4me3 and H3K27ac, which became more prominent only by the gastrula stage (Figure 3A, B). This early deposition and subsequent expansion of H3K27me3 likely contributes to the establishment of a transiently repressive chromatin environment that restrains premature activation of developmental genes, facilitating proper lineage specification. A comparable mechanism has been observed in zebrafish, where H3K27me3, sometimes co-occurring with H3K4me3, premarks homeostatic and developmental genes before ZGA onset (Lindeman et al., 2011). In addition, early signals of H3K4me1 and H3K27ac were detected from the 4-cell and morula stages, respectively, although their genomic distribution remained relatively limited until the gastrula stage (Figure 3A, B). These early-appearing active marks may serve

to prime key developmental loci for future transcriptional activation (Fukushima et al., 2023). Further functional investigation is required to clarify their specific roles during early embryogenesis.

Although chromatin remodeling during early embryogenesis is evolutionarily conserved, the timing and dynamics of histone modifications during the MZT vary considerably across species. In mammals, major ZGA occurs at the 2-cell stage in mice and the 8-cell stage in humans. Both repressive (H3K27me3) and activating histone marks (H3K4me3 and H3K27ac) are present prior to ZGA in these species, although their distribution patterns differ significantly: in mice, H3K27me3 is selectively removed from promoter regions while retained in the intergenic domains, whereas in humans, H3K27me3 is almost undetectable during ZGA but re-establishes later (Sotomayor-Lugo et al., 2024; Wu et al., 2023; Xia et al., 2019; Xu et al., 2021). In non-mammalian vertebrates such as zebrafish and medaka (*Oryzias latipes*), histone modifications undergo extensive reprogramming post-fertilization and are re-established around ZGA (Fukushima et al., 2023; Hickey et al., 2022; Zhang et al., 2018). In zebrafish, ZGA coincides with the mid-blastula transition (~10th cleavage), during which H3K4me3 is pre-deposited at promoters of key genes, while H3K27me3 marks only a small subset of loci before ZGA and expands afterward to facilitate lineage-specific repression (Duval et al., 2024; Hickey et al., 2022; Laue et al., 2019; Lindeman et al., 2011). In medaka, ZGA begins at the early blastula stage, but histone modification reprogramming remains incomplete: maternal H3K27ac, H3K27me3, and H3K9me3 persist through early cleavage, whereas H3K4 methylation is fully erased post-fertilization and is not restored until the late morula stage (Fukushima et al., 2023).

Among invertebrates, chromatin dynamics during the MZT also vary substantially. In *Drosophila melanogaster*, H3K4me1 and H3K4me3 are largely absent prior to major ZGA (nuclear cycle 14), while maternally inherited H3K27me3 persists at low levels throughout early cleavage and functions to restrict enhancer activity during the MZT (Ciabrelli et al., 2024; Zenk et al., 2017). In *Caenorhabditis elegans*, both H3K27me3 and H3K4me3 are inherited from parental genomes and maintained at relatively high levels during early development. During ZGA, H3K27me3 remains uniformly distributed across cells, whereas H3K4me3 exhibits lineage-specific accumulation (Jash & Csankovszki, 2024; Millán-Zambrano et al., 2022).

Studies examining histone modification dynamics in bivalves remain scarce, particularly using high-resolution techniques. In *C. gigas* (Pacific oyster), H3K4me1 and H3K27me3 are maintained from the 4–8 cell stage through the D-shaped larval stage, while H3K4me3 peaks at the 4–8 cell stage, followed by a sharp decline at the morula stage before

Table 1 Comparative overview of zygotic genome activation (ZGA) timing and chromatin modification dynamics across metazoan species

Species	Major ZGA timing	Histone modification characteristics	References
Mus musculus (mouse)	2-cell stage (~24 hpf)	Maternally inherited ncH3K4me3 replaced gradually by cH3K4me3 during ZGA; H3K27me3 cleared on promoters but retained in distal regions during ZGA; H3K4me3 and H3K27me3 prime developmental genes post-ZGA	Schulz & Harrison, 2019; Sotomayor-Lugo et al., 2024; Xu et al., 2021
Homo sapiens (human)	8-cell stage (72 hpf)	Prior to ZGA, cH3K4me3 is enriched at a large number of promoters and distal regulatory elements; H3K27me3 undergoes global depletion pre-ZGA but is re-established at developmental genes after ZGA	Sotomayor-Lugo et al., 2024; Wu et al., 2023; Xia et al., 2019
Danio rerio (zebrafish)	cell cycle 10 (~3.5 hpf)	H3K4me3 is pre-deposited at promoters before ZGA; H3K27me3 and H3K9me3 gradually accumulate after ZGA, contributing to chromatin compaction and lineage-specific regulation.	Duval et al., 2024; Hickey et al., 2022; Laue et al., 2019; Lindeman et al., 2011
Oryzias latipes (medaka)	Early blastula (~1 000 cells, ~6 hpf)	H3K27ac is detected as early as the 16-cell stage; partial retention of H3K27me3 at key developmental genes; H3K9me3 is retained at telomeric regions; H3K4me1/2/3 reaccumulate during ZGA after clearance.	Fukushima et al., 2023
Drosophila melanogaster	Nuclear cycle 14 (~2.5 hpf)	Intergenerationally inherited H3K27me3 and H3K9me3 establish a repressive background early; H3K27ac detected at low levels early, increasing at ZGA; H3K4me1, H3K4me3, and H3K9ac are up-regulated during ZGA.	Ciabrelli et al., 2024
Caenorhabditis elegans	Cell cycle 3 (~1.6 hpf)	H3K27me3 is parentally inherited and propagated during early development; H3K4me3 presents at high levels in early stages and accumulates in a lineage-specific manner during ZGA.	Jash & Csankovszki, 2024; Millán-Zambrano et al., 2022
Crassostrea gigas (Pacific oyster)	Not explicitly defined	H3K4me1 and H3K27me3 persist from 4–8 cell stages to D-larval stage; H3K4me3 peaks at 4–8 cell stage and decreases during morula stage; H3K9me1/3 decline and slightly rebound; global H3K27me levels remain stable.	Fellous et al., 2019
Patinopecten yessoensis (Japanese scallop)	Not explicitly defined; likely between 2–8 cell (~2–3 hpf) and gastrula stages (~20 hpf)	Multiple *Kdm* genes are highly expressed at the 2–8 cell stage; demethylases such as Kdm5, Kdm6, and Jarid2 show marked up-regulation during blastula and gastrula stages.	Guo et al., 2020
Mulinia lateralis (dwarf surf clam)	Around blastula (~4 hpf)	Histone modifications are nearly undetectable (with only a few H3K4me1 sites) before 4-cell stage. By the morula stage, H3K27me3 becomes relatively widespread, while permissive histone modifications (H3K4me1 and H3K27ac) start to emerge but at a less extent. At the blastula stage, H3K4me3 starts to accumulate and H3K27me3 propagates further and remains stable thereafter.	This study

c/ncH3K4me3: Canonical/non-canonical H3K4me3.

stabilizing (Fellous et al., 2019). These observations suggest that chromatin states are established earlier and remain comparatively stable in *C. gigas* compared to *M. lateralis*. In contrast, the scallop (*Patinopecten yessoensis*) shows pronounced histone demethylation across developmental stages, indicating continuous chromatin remodeling (Guo et al., 2020). These interspecies differences may reflect divergent developmental strategies or methodological variations, as earlier studies employed global methylation assays, while the present study utilized CUT&Tag, providing higher-resolution insights into chromatin state transitions. To facilitate cross-species comparisons, the timing of ZGA and corresponding histone modification patterns across selected species are summarized in Table 1.

Taken together, histone modification dynamics observed in *M. lateralis* most closely resemble those reported in *Drosophila*, with weak histone signals preceding ZGA and progressive establishment of both repressive (H3K27me3) and permissive (H3K4me1, H3K4me3, and H3K27ac) marks during genome activation. Notably, the earlier and broader establishment of H3K27me3 relative to activating modifications may represent a distinctive regulatory feature in *M. lateralis*, potentially reflecting a lineage-specific chromatin priming strategy.

CONCLUSIONS

This study provides a comprehensive analysis of histone modification dynamics and transcriptomic reprogramming during *M. lateralis* embryogenesis, elucidating key regulatory features associated with ZGA and developmental progression. H3K27me3 emerged as a repressive chromatin mark deposited early in development, likely mediated by EZH2-containing PRC2, and became broadly established prior to the widespread accumulation of permissive modifications such as H3K4me3, H3K27ac, and H3K4me1. These early-deposited histone modifications may facilitate the spatiotemporal coordination of developmental gene activation across distinct cell lineages during later embryogenesis.

Chromatin state profiling enabled the identification of cis-regulatory elements, while integrative analysis of actively transcribing genes revealed enrichment in key developmental signaling pathways, including Hippo, WNT, MAPK, and biomineralization. Core regulators such as *yap1*, *ppp2r1b*, *mtor*, and *smad4* were implicated as transcriptionally active during specific stages, underscoring their roles in lineage specification and morphogenesis. These findings establish a foundational epigenomic framework for *M. lateralis*, advancing bivalve developmental genomics and contributing to broader applications in evolutionary epigenetics and aquaculture.

Future studies should incorporate functional validation using targeted perturbation approaches, such as CRISPR-mediated editing, single-cell epigenomic profiling (e.g., single-cell CUT&Tag, ATAC-seq), and chromatin accessibility assays to resolve the causal roles of histone modifications in early development. Cross-species comparative analyses will provide deeper insights into the evolutionary diversity of chromatin regulation among marine invertebrates. By integrating molecular developmental biology with genome-wide epigenetics, this study establishes *M. lateralis* as a valuable model for studying histone modification reprogramming and the evolution of cis-regulatory architecture in non-model marine taxa.

DATA AVAILABILITY

The CUT&Tag and RNA-seq data generated in this study have been submitted to the NCBI database (BioProjectID PRJNA1224210 and PRJNA1257552), Genome Sequence Archive in National Genomics Data Center, China National Center for Bioinformation/Beijing Institute of Genomics, Chinese Academy of Sciences (https://ngdc.cncb.ac.cn/gsa) under accession numbers CRA045750 and CRA045756, and Science Data Bank (CSTR:31253.11.sciencedb.j00139.00243 for CUT&Tag data and CSTR:31253.11.sciencedb.j00139.00244 for RNA-seq data). The supplementary file containing the chromHMM output files can be downloaded from figshare via https://doi.org/10.6084/m9.figshare.28418309.v2.

SUPPLEMENTARY DATA

Supplementary data to this article can be found online.

COMPETING INTERESTS

The authors declare that they have no competing interests.

AUTHORS' CONTRIBUTIONS

Z.Y. and J.L.S. conceived the study. Z.Y., J.J.H., and Z.M.B. supervised the study. Z.Y. and J.L.S. designed the experiments. J.L.S. and M.M.Y. performed the experiments. J.L.S., J.X.L., and Z.C.W. performed the data analysis and visualization. Z.J.Y. provided technical support. Z.Y., J.J.H., and Z.M.B. provided funding support. Z.Y. and J.L.S. wrote the draft manuscript. All authors read and approved the final version of the manuscript.

ACKNOWLEDGMENTS

We acknowledge the support of the High-Performance Biological Supercomputing Center at the Ocean University of China for this research.

REFERENCES

Bae S, Lesch BJ. 2020. H3K4me1 distribution predicts transcription state and poising at promoters. *Frontiers in Cell and Developmental Biology*, **8**: 289.

Bannister AJ, Kouzarides T. 2011. Regulation of chromatin by histone modifications. *Cell Research*, **21**(3): 381–395.

Banović Đeri B, Nešić S, Vićić I, et al. 2024. Benchmarking of five NGS mapping tools for the reference alignment of bacterial outer membrane vesicles-associated small RNAs. *Frontiers in Microbiology*, **15**: 1401985.

Bartosovic M, Kabbe M, Castelo-Branco G. 2021. Single-cell CUT&Tag profiles histone modifications and transcription factors in complex tissues. *Nature Biotechnology*, **39**(7): 825–835.

Beadle LF, Love JC, Shapovalova Y, et al. 2023. Combined modelling of mRNA decay dynamics and single-molecule imaging in the *Drosophila* embryo uncovers a role for P-bodies in 5′ to 3′ degradation. *PLoS Biology*, **21**(1): e3001956.

Blayney JW, Francis H, Rampasekova A, et al. 2023. Super-enhancers include classical enhancers and facilitators to fully activate gene expression. *Cell*, **186**(26): 5826–5839. e18.

Boileau RM, Chen KX, Blelloch R. 2023. Loss of *MLL3/4* decouples enhancer H3K4 monomethylation, H3K27 acetylation, and gene activation during embryonic stem cell differentiation. *Genome Biology*, **24**(1): 41.

Bolar NA, Golzio C, Živná M, et al. 2016. Heterozygous loss-of-function *SEC61A1* mutations cause autosomal-dominant tubulo-interstitial and glomerulocystic kidney disease with anemia. *The American Journal of Human Genetics*, **99**(1): 174–187.

Brahma S, Henikoff S. 2024. The BAF chromatin remodeler synergizes with RNA polymerase II and transcription factors to evict nucleosomes. *Nature Genetics*, **56**(1): 100–111.

Brandmann T, Fakim H, Padamsi Z, et al. 2018. Molecular architecture of

LSM14 interactions involved in the assembly of mRNA silencing complexes. *The EMBO Journal*, **37**(17): e97869.

Chirichella M, Bianchi N, Džafo E, et al. 2022. RFX transcription factors control a miR-150/PDAP1 axis that restrains the proliferation of human T cells. *PLoS Biology*, **20**(2): e3001538.

Ciabrelli F, Atinbayeva N, Pane A, et al. 2024. Epigenetic inheritance and gene expression regulation in early Drosophila embryos. *EMBO Reports*, **25**(10): 4131–4152.

Crespo M, Damont A, Blanco M, et al. 2020. Multi-omic analysis of gametogenesis reveals a novel signature at the promoters and distal enhancers of active genes. *Nucleic Acids Research*, **48**(8): 4115–4138.

Dobin A, Davis CA, Schlesinger F, et al. 2013. STAR: ultrafast universal RNA-seq aligner. *Bioinformatics*, **29**(1): 15–21.

Drozdov A, Lebedev E, Adonin L. 2023. Comparative analysis of bivalve and sea urchin genetics and development: investigating the dichotomy in Bilateria. *International Journal of Molecular Sciences*, **24**(24): 17163.

Duval KL, Artis AR, Goll MG. 2024. The emerging H3K9me3 chromatin landscape during zebrafish embryogenesis. *Genetics*, **228**(2): iyae138.

Eichten SR, Schmitz RJ, Springer NM. 2014. Epigenetics: beyond chromatin modifications and complex genetic regulation. *Plant Physiology*, **165**(3): 933–947.

Ernst J, Kellis M. 2017. Chromatin-state discovery and genome annotation with ChromHMM. *Nature Protocols*, **12**(12): 2478–2492.

Fallet M, Luquet E, David P, et al. 2020. Epigenetic inheritance and intergenerational effects in mollusks. *Gene*, **729**: 144166.

Fellous A, Le Franc L, Jouaux A, et al. 2019. Histone methylation participates in gene expression control during the early development of the Pacific oyster *Crassostrea gigas*. *Genes*, **10**(9): 695.

Feng JX, Liu T, Qin B, et al. 2012. Identifying ChIP-seq enrichment using MACS. *Nature Protocols*, **7**(9): 1728–1740.

Food and Agriculture Organization of the United Nation (FAO). 2024. The state of food security and nutrition in the world 2024: financing to end hunger, food insecurity and malnutrition in all its forms. Rome: FAO Report, 246.

Fukushima HS, Takeda H, Nakamura R. 2023. Incomplete erasure of histone marks during epigenetic reprogramming in medaka early development. *Genome Research*, **33**(4): 572–586.

Guo XL, Li XX, Zhao F, et al. 2023. Full-length transcriptome analysis provides insights into larval shell formation in *Mulinia lateralis*. *Frontiers in Marine Science*, **9**: 1111241.

Guo ZY, Zhang LJ, Li YJ, et al. 2020. Expression profiling of the *Kdm* genes in scallop *Patinopecten yessoensis* suggests involvement of histone demethylation in regulation of early development and gametogenesis. *Comparative Biochemistry and Physiology Part B: Biochemistry and Molecular Biology*, **243**–**244**: 110434.

Hanna CW, Huang JH, Belton C, et al. 2022. Loss of histone methyltransferase SETD1B in oogenesis results in the redistribution of genomic histone 3 lysine 4 trimethylation. *Nucleic Acids Research*, **50**(4): 1993–2004.

Hickey GJ, Wike CL, Nie XC, et al. 2022. Establishment of developmental gene silencing by ordered polycomb complex recruitment in early zebrafish embryos. *eLife*, **11**: e67738.

Jash E, Csankovszki G. 2024. Chromatin organization during *C. elegans* early development. *DNA*, **4**(1): 64–83.

Jiao LY, Liu X. 2015. Structural basis of histone H3K27 trimethylation by an active polycomb repressive complex 2. *Science*, **350**(6258): aac4383.

Kaya-Okur HS, Janssens DH, Henikoff JG, et al. 2020. Efficient low-cost chromatin profiling with CUT&Tag. *Nature Protocols*, **15**(10): 3264–3283.

Kaya-Okur HS, Wu SJ, Codomo CA, et al. 2019. CUT&Tag for efficient epigenomic profiling of small samples and single cells. *Nature Communications*, **10**(1): 1930.

Kranz A, Anastassiadis K. 2020. The role of SETD1A and SETD1B in development and disease. *Biochimica et Biophysica Acta (BBA) - Gene Regulatory Mechanisms*, **1863**(8): 194578.

Langfelder P, Horvath S. 2008. WGCNA: an R package for weighted correlation network analysis. *BMC Bioinformatics*, **9**(1): 559.

Laue K, Rajshekar S, Courtney AJ, et al. 2019. The maternal to zygotic transition regulates genome-wide heterochromatin establishment in the zebrafish embryo. *Nature Communications*, **10**(1): 1551.

Lawrence M, Huber W, Pagès H, et al. 2013. Software for computing and annotating genomic ranges. *PLoS Computational Biology*, **9**(8): e1003118.

Letunic I, Bork P. 2021. Interactive Tree of Life (iTOL) v5: an online tool for phylogenetic tree display and annotation. *Nucleic Acids Research*, **49**(W1): W293–W296.

Li H. 2013. Aligning sequence reads, clone sequences and assembly contigs with BWA-MEM. *arXiv*, doi: https://doi.org/10.48550/arXiv.1303.3997

Li H, Durbin R. 2009. Fast and accurate short read alignment with Burrows-Wheeler transform. *Bioinformatics*, **25**(14): 1754–1760.

Liao Y, Smyth GK, Shi W. 2014. featureCounts: an efficient general purpose program for assigning sequence reads to genomic features. *Bioinformatics*, **30**(7): 923–930.

Lindeman LC, Andersen IS, Reiner AH, et al. 2011. Prepatterning of developmental gene expression by modified histones before zygotic genome activation. *Developmental Cell*, **21**(6): 993–1004.

Linxweiler M, Schick B, Zimmermann R. 2017. Let's talk about Secs: Sec61, Sec62 and Sec63 in signal transduction, oncology and personalized medicine. *Signal Transduction and Targeted Therapy*, **2**(1): 17002.

Liu BF, He YL, Wu XT, et al. 2024. Mapping putative enhancers in mouse oocytes and early embryos reveals TCF3/12 as key folliculogenesis regulators. *Nature Cell Biology*, **26**(6): 962–974.

Liu G, Huan P, Liu BZ. 2014. Cloning and expression patterns of two *Smad* genes during embryonic development and shell formation of the Pacific oyster *Crassostrea gigas*. *Chinese Journal of Oceanology and Limnology*, **32**(6): 1224–1231.

Love MI, Huber W, Anders S. 2014. Moderated estimation of fold change and dispersion for RNA-seq data with DESeq2. *Genome Biology*, **15**(12): 550.

Lu T, Ang CE, Zhuang XW. 2022. Spatially resolved epigenomic profiling of single cells in complex tissues. *Cell*, **185**(23): 4448–4464. e17.

Meléndez García R, Haccard O, Chesneau A, et al. 2022. A non-transcriptional function of Yap regulates the DNA replication program in *Xenopus laevis*. *eLife*, **11**: e75741.

Millán-Zambrano G, Burton A, Bannister AJ, et al. 2022. Histone post-translational modifications—cause and consequence of genome function. *Nature Reviews Genetics*, **23**(9): 563–580.

Patel RK, Jain M. 2012. NGS QC Toolkit: a toolkit for quality control of next generation sequencing data. *PLoS One*, **7**(2): e30619.

Pecori F, Torres-Padilla ME. 2023. Dynamics of nuclear architecture during early embryonic development and lessons from liveimaging. *Developmental Cell*, **58**(6): 435–449.

Pekowska A, Benoukraf T, Zacarias-Cabeza J, et al. 2011. H3K4 tri-methylation provides an epigenetic signature of active enhancers. *The EMBO Journal*, **30**(20): 4198–4210.

Pinello L, Xu J, Orkin SH, et al. 2014. Analysis of chromatin-state plasticity identifies cell-type-specific regulators of H3K27me3 patterns. *Proceedings of the National Academy of Sciences of the United States of America*, **111**(3): E344–E353.

Quinlan AR. 2014. BEDTools: the Swiss-Army tool for genome feature analysis. *Current Protocols in Bioinformatics*, **47**: 11.12. 1–11.12. 34.

Rivera-Casas C, Gonzalez-Romero R, Garduño RA, et al. 2017. Molecular and biochemical methods useful for the epigenetic characterization of

chromatin-associated proteins in bivalve molluscs. *Frontiers in Physiology*, **8**: 490.

Roadmap Epigenomics Consortium, Kundaje A, Meuleman W, et al. 2015. Integrative analysis of 111 reference human epigenomes. *Nature*, **518**(7539): 317–330.

Schultz J, Milpetz F, Bork P, et al. 1998. SMART, a simple modular architecture research tool: identification of signaling domains. *Proceedings of the National Academy of Sciences of the United States of America*, **95**(11): 5857–5864.

Schulz KN, Harrison MM. 2019. Mechanisms regulating zygotic genome activation. *Nature Reviews Genetics*, **20**(4): 221–234.

Seshacharyulu P, Pandey P, Datta K, et al. 2013. Phosphatase: PP2A structural importance, regulation and its aberrant expression in cancer. *Cancer Letters*, **335**(1): 9–18.

Shen MH, Di GL, Li M, et al. 2018. Proteomics studies on the three larval stages of development and metamorphosis of *Babylonia areolata*. *Scientific Reports*, **8**(1): 6269.

Sotomayor-Lugo F, Iglesias-Barrameda N, Castillo-Aleman YM, et al. 2024. The dynamics of histone modifications during mammalian zygotic genome activation. *International Journal of Molecular Sciences*, **25**(3): 1459.

Stefano BD, Luo EC, Haggerty C, et al. 2019. The RNA helicase DDX6 controls cellular plasticity by modulating P-body homeostasis. *Cell Stem Cell*, **25**(5): 622–638. e13.

Subtelny AO, Eichhorn SW, Chen GR, et al. 2014. Poly(A)-tail profiling reveals an embryonic switch in translational control. *Nature*, **508**(7494): 66–71.

Sun L, Li XF, Luo H, et al. 2023. EZH2 can be used as a therapeutic agent for inhibiting endothelial dysfunction. *Biochemical Pharmacology*, **213**: 115594.

Tamura K, Stecher G, Kumar S. 2021. MEGA11: molecular evolutionary genetics analysis version 11. *Molecular Biology and Evolution*, **38**(7): 3022–3027.

Toyo-oka K, Shionoya A, Gambello MJ, et al. 2003. 14-3-3ε is important for neuronal migration by binding to NUDEL: a molecular explanation for Miller-Dieker syndrome. *Nature Genetics*, **34**(3): 274–285.

Turner BM. 2007. Defining an epigenetic code. *Nature Cell Biology*, **9**(1): 2–6.

Vastenhouw NL, Cao WX, Lipshitz HD. 2019. The maternal-to-zygotic transition revisited. *Development*, **146**(11): dev161471.

Vaughn CC, Hoellein TJ. 2018. Bivalve impacts in freshwater and marine ecosystems. *Annual Review of Ecology, Evolution, and Systematics*, **49**: 183–208.

Völkel P, Bary A, Raby L, et al. 2019. *Ezh1* arises from *Ezh2* gene duplication but its function is not required for zebrafish development. *Scientific Reports*, **9**(1): 4319.

Wang CF, Chen C, Liu XY, et al. 2022. Dynamic nucleosome organization after fertilization reveals regulatory factors for mouse zygotic genome activation. *Cell Research*, **32**(9): 801–813.

Wang J, Zhang LL, Lian SS, et al. 2020. Evolutionary transcriptomics of metazoan biphasic life cycle supports a single intercalation origin of metazoan larvae. *Nature Ecology & Evolution*, **4**(5): 725–736.

Weichhart T, Hengstschläger M, Linke M. 2015. Regulation of innate immune cell function by mTOR. *Nature Reviews Immunology*, **15**(10): 599–614.

Wickham H. 2011. Ggplot2. *WIREs Computational Statistics*, **3**(2): 180–185.

Wu KL, Fan DD, Zhao H, et al. 2023. Dynamics of histone acetylation during human early embryogenesis. *Cell Discovery*, **9**(1): 29.

Wu SJ, Furlan SN, Mihalas AB, et al. 2021. Single-cell CUT&Tag analysis of chromatin modifications in differentiation and tumor progression. *Nature Biotechnology*, **39**(7): 819–824.

Wu X, Heffelfinger C, Zhao HY, et al. 2019. Benchmarking variant identification tools for plant diversity discovery. *BMC Genomics*, **20**(1): 701.

Xia WK, Xu JW, Yu G, et al. 2019. Resetting histone modifications during human parental-to-zygotic transition. *Science*, **365**(6451): 353–360.

Xu RM, Li C, Liu XY, et al. 2021. Insights into epigenetic patterns in mammalian early embryos. *Protein & Cell*, **12**(1): 7–28.

Yang J, Liu MH, Shen WL, et al. 2022. H3K4me3 CUT&Tag and transcriptome analysis reveal the epigenetic regulatory landscape in gill tissue of large yellow croaker (*Larimichthys crocea*) under low salinity stress. *Frontiers in Marine Science*, **9**: 906337.

Yang ZJ, Huang XT, Wang H, et al. 2021. Effects of microalgae diets and stocking density on larval growth, survival and metamorphosis of dwarf surfclam, *Mulinia lateralis*. *Aquaculture*, **536**: 736440.

Ye Z, Braden CR, Wills A, et al. 2021. Identification of *in vivo Hox13*-binding sites reveals an essential locus controlling zebrafish *brachyury* expression. *Development*, **148**(11): dev199408.

Yu GC, Wang LG, Han YY, et al. 2012. clusterProfiler: an R package for comparing biological themes among gene clusters. *OMICS: A Journal of Integrative Biology*, **16**(5): 284–287.

Yu GC, Wang LG, He QY. 2015. ChIPseeker: an R/Bioconductor package for ChIP peak annotation, comparison and visualization. *Bioinformatics*, **31**(14): 2382–2383.

Yu Y, Li XJ, Jiao R, et al. 2023. H3K27me3-H3K4me1 transition at bivalent promoters instructs lineage specification in development. *Cell & Bioscience*, **13**(1): 66.

Zenk F, Loeser E, Schiavo R, et al. 2017. Germ line-inherited H3K27me3 restricts enhancer function during maternal-to-zygotic transition. *Science*, **357**(6347): 212–216.

Zhang BJ, Wu XT, Zhang WH, et al. 2018. Widespread enhancer dememorization and promoter priming during parental-to-zygotic transition. *Molecular Cell*, **72**(4): 673–686. e6.

Zhang W, Liu HT. 2002. MAPK signal pathways in the regulation of cell proliferation in mammalian cells. *Cell Research*, **12**(1): 9–18.

Zhao M, Shi Y, He MX, et al. 2016. *PfSMAD4* plays a role in biomineralization and can transduce bone morphogenetic protein-2 signals in the pearl oyster *Pinctada fucata*. *BMC Developmental Biology*, **16**(1): 9.

Zheng QW, Wu XT, Li X, et al. 2024. Low-input CUT&Tag for efficient epigenomic profiling of zebrafish stage I oocytes. *Frontiers in Cell and Developmental Biology*, **12**: 1475912.

Zhu W, Xu XC, Wang XX, et al. 2019. Reprogramming histone modification patterns to coordinate gene expression in early zebrafish embryos. *BMC Genomics*, **20**(1): 248.

Zhu Y, Li WN, Dong YF, et al. 2023. *C. elegans* hemidesmosomes sense collagen damage to trigger innate immune response in the epidermis. *Cells*, **12**(18): 2223.

Zinski J, Tajer B, Mullins MC. 2018. TGF-β family signaling in early vertebrate development. *Cold Spring Harbor Perspectives in Biology*, **10**(6): a033274.